Coatings **2014**, *4*, 253-281; doi:10.3390/coatings4020253

OPEN ACCESS

coatings

ISSN 2079-6412

www.mdpi.com/journal/coatings

Article

Completely Analytical Tools for the Next Generation of Surface and Coating Optimization

Norbert Schwarzer

Saxonian Institute of Surface Mechanics (SIO), Tankow 2, 18569 Ummanz, Germany;
E-Mail: n.schwarzer@siomec.de; Tel.: +49-38305-529842; Fax: +49-38305-529842-9

Received: 14 March 2014; in revised form: 9 April 2014 / Accepted: 15 April 2014 / Published: 23 April 2014

Abstract: Usually, some severe efforts are required to obtain tribological parameters like Archard's wear depth parameter k_d. Complex tribological experiments have to be performed and analyzed. The paper features an approach where such parameters are extracted from effective interaction potentials in combination with more physical-oriented measurements, such as Nanoindentation and physical scratch. Thereby, the effective potentials are built up and fed from such tests. By using effective material potentials one can derive critical loading situations leading to failure (decomposition strength) for any contact situation. A subsequent connection of these decomposition or failure states with the corresponding stress or strain distributions allows the development of rather comprehensive tribological parameter models, applicable in wear and fatigue simulations, as demonstrated in this work. From this, a new relatively general wear model has been developed on the basis of the effective indenter concept by using the extended Hertzian approach for a great variety of loading situations. The models do not only allow to analyze certain tribological experiments, such as the well known pin-on disk test or the more recently developed nano-fretting test, but also to forward simulate such tests and even give hints for structured optimization or result in better component life-time prediction. The work will show how the procedure has to be applied in general and a small selection of practical examples will be presented.

Keywords: effective potentials; first principles; indentation; contact experiments; viscoelastic properties; polymers; layered structures; optimized coatings

1. Introduction

In order to achieve the goal set in the headline, namely, to analytically optimize surface and coating structures, which includes the extraction of generic tribological or wear parameters, it is necessary to combine quite a few fields and/or concepts of material science. Therefore, this introduction needs to cover the following issues:

- first principle based effective interatomic potential description of mechanical material behavior [1] and its extension into the time-domain [2];
- the effective indenter concept [3–6], made time dependent;
- the extension of the Oliver and Pharr method to analyze nanoindentation data to layered materials and time dependent mechanical behavior [7–10];
- the physical scratch and/or tribological test and its analysis [11–14].

1.1. Simple First Principle Based Interatomic Potential Description of Mechanical Material Behavior

It was shown in [15] that on the basis of an effective potential function like the Morse potential given as

$$V_{\mathrm{Morse}} = \varepsilon\left[\mathrm{e}^{-2p(r-r_0)} - 2\mathrm{e}^{-p(r-r_0)}\right] \tag{1}$$

A contact problem can be evaluated using the mechanical parameters derived from such a potential. Here, p, ε, σ are material parameters and r_0 usually denotes the equilibrium bond length. In such a case, the potential would define the pair interaction. Here, however, as in [1,15], we will apply the potential as an effective one with r_0 denoting the lattice constant (see also [16]). With respect to molecular dynamic simulation such an effective potential could be the basis for the extraction of the necessary pair and higher order interactions as demonstrated in [16]. For our study, however, we will not need this, because we are only interested in the mechanical constants, especially the Young's modulus and the decomposition strength. Having this, one can apply the method described in [15] to simulate a mechanical contact problem, thereby even taking nonlinear effects like the pressure, shear and temperature dependency of the Young's modulus, and other mechanical constants into account [2]. We will show that especially within tribological applications temperature fields can play an important role in influencing the mechanical properties of the material.

1.2. Brief Story about the "Effective Indenter Concept" and Its Extension to Layered Materials

"Surface" usually is not "bulk" and, so, subsequently, the behavior of surfaces, especially their mechanical behavior can be dramatically different from what one might expect by just applying bulk concepts to surface problems, such as contact situations with very surface-located, surface-dominated stress and strain fields. In tribo and wear problems, this very often compromises our ability to simulate and understand the physical processes taking place in certain tests (e.g., [17–21]). In order to improve this situation we, therefore, resort to a stringent application of a layered material model considering and modeling the mechanical surface always as—at least potentially—having a property profile starting from the mechanical bulk values in depth usually well known for a certain material to rather often completely different properties on the top-most surface layer. In the case of coated materials this model extension, of course, can easily be justified by the explicit coating structure. However, we should stress

the point of also carefully and critically considering apparent "homogenous surfaces" as—rather often—being of gradient or somehow layered character. In addition tribological applications often come with temperature fields due to friction, be it the internal friction caused by shear stresses or the external one coming from the multiple tribological contact situations. As shown in [2], such temperature fields can couple back into the mechanical properties influencing the tribological contact conditions.

The "effective indenter concept" itself can mathematically be described or understood as some kind of quasi conform coordinate transformation transforming the difficult problem of a curved surface contacted by a well defined indenter (like a cone) into a flat surface loaded with a complexly formed indenter. Already, in 1994, Bolshakov, Oliver, and Pharr [3] introduced this "Concept of the Effective Indenter" and refined it in a series of wonderful publications until, in 2002, the paper about "Understanding of nanoindentation unloading curves" [4] was published by Pharr and Bolshakov.

The extension of this concept is simply performed by substituting the homogenous half space model describing the loaded sample body by a layered half space model [22].

1.3. About the Extension of the Oliver and Pharr Method to Analyze Nanoindentation Data of Layered Materials and Time Dependent Mechanical Behavior

As it is a well established fact, that the classical Oliver and Pharr method [7], as an approach based upon the homogenous half space model, cannot directly be applied to layered materials and small structures, the author here refers to the literature (e.g., [23]). Soon after the publication of the Oliver and Pharr method it became clear that there is a physical concept on which this method can be based. It was called the "Concept of the Effective Indenter" [3,4]. During a small conference in Italy in 1999, the author learned of that concept and decided to work out a theory solving not only the problem for the mechanical contact of an indenter with general shape of symmetry of revolution, but also to extend this solution to layered structures [24]. Later on, he also presented a variety of applications together with Pharr, Chudoba, Richter and others [5,6,8,9,25–27]. Soon, it became clear, however, that the "effective indenter theory", even though powerful, was not something one could easily give to the engineer or an indenter experimentalist and expect her or him to use it as a tool for the analysis of indentation data. The reason for this lays in the complexity of the formulae building the solution. Thus, the whole approach was brought into a software package named FilmDoctor® [28].

Making the Classical Oliver and Pharr Method Fit for Time Dependent Mechanical Behavior

In an indentation test we always find complex three-dimensional stress states with usually all stress components being non-zero. Thus, as Fischer-Cripps put it, "the nature of the loading is a complex mixture of hydrostatic compression, tension, and shear" [29]. In the case of viscous behavior we also have to understand that we even have complex mixtures of stress and strain rates. These however, usually influence the time dependent mechanical parameters [30]. This automatically means that at different positions we find different stress and strain states and rates subsequently leading to different mechanical parameters (time dependent) at different positions within the material. This automatically makes the system of usually linear partial differential equations of Elasticity non-linear in the moment viscosity (even elastic viscosity) comes into play. In order to keep things simple, however, we will not go here for a non-linear basic solution, but try to find effective, phenomenological descriptions for

visco-elastic, visco-plastic contact problems, based on the concept of a time dependent effective indenter. As an additional difficulty coming into play especially in connection with tribological applications we again have to consider temperature fields possibly influencing the mechanical parameters. It was shown in [2] that even smallest temperature gradients can have a dramatic influence and as tribological contacts usually and mainly inevitably produce heat this effect cannot be ignored when trying to physically simulate tribo experiments.

1.4. Introduction into the Physical Scratch and/or Tribological Test and Its Analysis

The standard scratch test is a widely used method to test the mechanical stability of coatings on different types of substrates and has become a sensitive technique to control the reliability of the manufacturing process. It is based on various standards [31,32].

Unfortunately, these standards do not allow to design and/or perform the tests in a truly physical way, meaning to extract generic physical parameters being later applicable in life-time prediction and optimization. For this, a more sophisticated approach is required, which assures physical parameter identification at each and every step towards physical tribological tests. The procedure is outlined in Figure 1.

Following the flowchart in Figure 1 we have started our surface characterization process with nanoindentation. The section above covered the calculation of true mechanical (potentially layered) surface properties out of these nanoindentation tests. Thus, now all mechanical values are known which are not only required to properly dimension (fine-tune) a scratch or tribology test for specific surface structures, but also are of need for a physical analysis of these tests. Again the flow chart (Figure 1) might give an illustrative understanding into such a test procedure.

The reader will find illustrative examples and a much more comprehensive elaboration of the method elsewhere [11–14].

Figure 1. A flow chart of the procedure of mechanical characterization and optimization of arbitrary structured surfaces with respect to wear and fretting. See references about features and tools [28,33–36] been given in the flow chart.

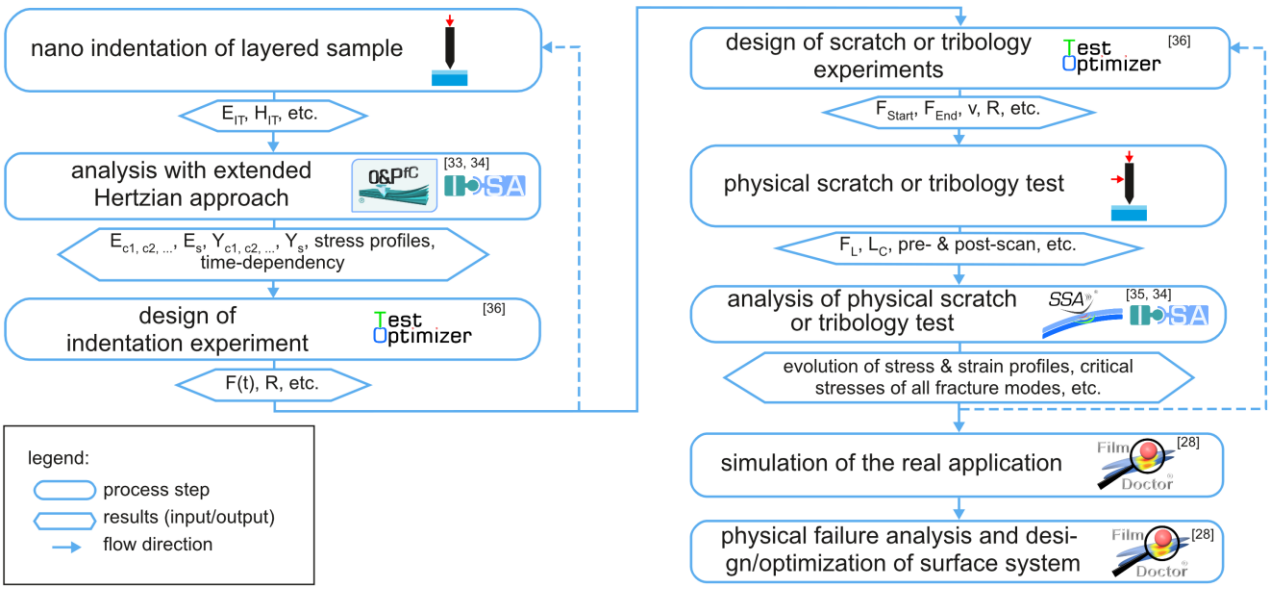

2. Theory Section

2.1. First Principle Based Interatomic Potential Description of Mechanical Material Behavior

As shown in [1], the pressure P and bulk modulus B can be derived from an effective potential. Thereby it is convenient to express P and B in units of B_0 (B at $P = 0$). By substituting the lattice distance r by $r = \mathrm{c} \times r_0$, P and B result in the relations:

$$\begin{aligned} {}^{P}\!/_{B_0} &= \tfrac{\mathrm{e}^{r_0 p(1-c)}}{r_0 p c^2}\left[1 - \mathrm{e}^{r_0 p(1-c)}\right]; \\ {}^{B}\!/_{B_0} &= \tfrac{\mathrm{e}^{r_0 p(1-c)}}{r_0 p c^2}\left[2(1 + r_0 p c)\mathrm{e}^{r_0 p(1-c)} - 2 - r_0 p c\right] \end{aligned} \tag{2}$$

As estimates for the critical r leading to decomposition (*cf.* [1]) we take the following expressions which have to be solved numerically ($r_{00} = p \times r_0$) to extract the critical c-value c_m for maximum $P(c)$:

$$6(1 + c_\mathrm{m} r_{00}) - 3\mathrm{e}^{r_{00}(c_\mathrm{m}-1)}(2 + c_\mathrm{m} r_{00}) = 0 \tag{3}$$

As a purely mathematically based measure for the critical bond length or in our case of an effective potential the lattice distance, the inflexion point for $c_\mathrm{ifp} > c_\mathrm{m}$ could be used. This can be numerically obtained for the Morse potential via:

$$6 + c_\mathrm{ifp} r_{00}\left(4 + c_\mathrm{ifp} r_{00}\right) - 2\mathrm{e}^{r_{00}\left(1-c_\mathrm{ifp}\right)}\left(3 + 2c_\mathrm{ifp} r_{00}(2 + c_\mathrm{ifp} r_{00})\right) = 0 \tag{4}$$

As shown in [2], the presence of deviatoric or shear stress components reduces the theoretical strength towards tension by up to 10%. This is of special importance for multiaxial contact situations where the stress tensor always is of mixed form and fully filled.

One also needs to check for temperature gradients caused by external and internal friction due to the tribological shear. It was shown in [2] that, caused by the inhomogeneity of the temperature $T(t,r)$ and subsequently the relaxation $\tau(t,r)$ field, an originally simple approach for the bond interaction, e.g., the Standard Linear Solid (SLS) becomes rather complicated regarding its bulk modulus behavior. Here, t and r are denoting time and space coordinates, respectively. Instead of a phenomenological SLS with the well known bulk modulus of the kind:

$$\begin{aligned} B_0 &= \frac{c}{18N} f^2 \left\{ \left[\sum_{\forall j, j \neq i} \left. \frac{\mathrm{d}^2 V_j\left(\tilde{r}_{ij}\right)}{\mathrm{d}\tilde{r}_{ij}^2} \right|_{r_{ij} = r_{0ij}} \right] \frac{1}{r_{0ij}} \right\} \\ &= \frac{c}{18N}\left(E_0 + E_1 \mathrm{e}^{\frac{-t}{\tau}}\right) \left\{ \left[\sum_{\forall j, j \neq i} \left. \frac{\mathrm{d}^2 V_j\left(\tilde{r}_{ij}\right)}{\mathrm{d}\tilde{r}_{ij}^2} \right|_{r_{ij} = r_{0ij}} \right] \frac{1}{r_{0ij}} \right\} \end{aligned} \tag{5}$$

(N gives the number of particles and c defines a parameter connected with the volume of an individual particle) and a subsequent Young's modulus time dependency like $E_0 + E_1 \mathrm{e}^{\frac{-t}{\tau}}$ we have a resulting phenomenological Young's modulus structure of the form:

$$E(t) = E_0 + E_1 \mathrm{e}^{\frac{-t}{\tau(T_j(r,z),\mu)}} + \vec{r} \cdot E_1 \mathrm{e}^{\frac{-t}{\tau(T_j(r,z),\mu)}} \frac{t}{\tau^2} \frac{\mathrm{d}\tau}{\mathrm{d}\vec{r}} + \vec{r} \cdot \vec{r} \frac{\left(E_1 \mathrm{e}^{\frac{-t}{\tau(T_j(r,z),\mu)}} \frac{t}{\tau^2} \frac{\mathrm{d}\tau}{\mathrm{d}\vec{r}} \right)^2}{4 \left(E_0 + E_1 \mathrm{e}^{\frac{-t}{\tau(T_j(r,z),\mu)}} \right)} \quad (6)$$

With a known principle structure for the temperature distribution function deduced from the shear stress distribution (adiabatic approach) such an approach seems to be manageable by the means of iterations. With a typical dependency for the temperature dependent relaxation time like [37,38]:

$$\tau = {}^{\eta}/_{E_1} = \frac{\eta_0 \mathrm{e}^{W_\mathrm{A}/(k_\mathrm{B}T)}}{E_1} \quad (7)$$

(with a constant W_A and the $T = T_0$ – viscosity η_0 and the Boltzmann-constant k_B) one can evaluate the mechanical contact situations applying the techniques elaborated in [2] (theory part II) under the assumption of completely adiabatic temperature fields resulting from shear and completely following the second stress invariant distribution. Please note, the positive sign in the exponential function for the relaxation time assuring decreasing viscosity η with increasing temperature.

2.2. The Effective Indenter Concept

In order to have a sufficiently great variability for the definition of differently shaped "effective indenters", we apply the extended Hertzian approach as shown in [39] for instance. With this approach normal and even tangential load distributions of the form [24]:

$$\sigma_{zz0}(r,\varphi) = \sum_{n=0}^{N} c_{\sigma n} r^n \sqrt{a^2 - r^2} \quad (8)$$

$$\tau_{rz0}(r,\varphi) = \sum_{n=0}^{N} c_{\tau rn} r^n \sqrt{a^2 - r^2}$$

$$\tau_{xz0}(r,\varphi) = \sum_{n=0}^{N} c_{\tau xn} r^n \sqrt{a^2 - r^2} \quad (9)$$

$$\tau_{yz0}(r,\varphi) = \sum_{n=0}^{N} c_{\tau yn} r^n \sqrt{a^2 - r^2}$$

with n = 0, 2, 4, 6 and arbitrary constants c can be solved completely (by following the instructions of the mathematical procedures for obtaining the complete potential functions as given in [24] even arbitrarily high, but only even N).

Together with lateral loads (occurring in all scratch-, tribotesters, or the next generation of nanoindenters and their applications, see, e.g., [39–42]) one often faces tilting moments leading to a normal surface stress distribution of the form:

$$\sigma_{zz0}(r,\varphi) = \sum_{n=0}^{N} c_{\sigma n} r^{n+1} \cos(\varphi) \sqrt{a^2 - r^2} \quad (10)$$

These stresses can for example occur when the indenter shaft is dragged over the surface. As the shaft itself is elastic and, thus, would be bent during the lateral loading, an unavoidable tilting moment results

and acts on the contacted surface. In addition, curved surfaces (e.g., due to roughness) can lead to such tilting moments.

In order to simulate the internal complex material structure of porous or composite materials, certain defect fields must be developed and combined with the external loads. Such fields can be extracted from the mathematical apparatus originally developed for the effective indenter contact by a simple generalization procedure. By developing such a defect model, one also obtains a very comprehensive tool for the construction of relatively general intrinsic stress distributions caused by internal inhomogeneities. Circular, disc-like inclusions could for example be simulated by the use of plane defects within the layered half space. Thus, introducing circular defects of radii a_i of the loading type:

$$\begin{aligned}\tau_{rz0}(r_i=\sqrt{(x-x_i)^2+(y-y_i)^2},z_i+0)&=\sum_{n=0}^{N}c_{\tau\,i,n}r_i^n\sqrt{a_i^2-r_i^2}\\ \tau_{rz0}(r_i=\sqrt{(x-x_i)^2+(y-y_i)^2},z_i-0)&=-\sum_{n=0}^{N}c_{\tau\,i,n}r_i^n\sqrt{a_i^2-r_i^2}\end{aligned}\tag{11}$$

$$\begin{aligned}\sigma_{zz0}(r_i=\sqrt{(x-x_i)^2+(y-y_i)^2},z_i+0)&=\sum_{n=0}^{N}c_{\sigma\,i,n}r_i^n\sqrt{a_i^2-r_i^2}\\ \sigma_{zz0}(r_i=\sqrt{(x-x_i)^2+(y-y_i)^2},z_i-0)&=-\sum_{n=0}^{N}c_{\sigma\,i,n}r_i^n\sqrt{a_i^2-r_i^2}\end{aligned}\tag{12}$$

(with x_i, y_i, z_i denoting the center of the defect and n = 0, 2, 4, 6) directly allows us the application of the extended Hertzian approach [24] that provides a complete solution of the elastic field of the defect loading given above. By superposing a multitude of such "defect dots", one could model (simulate) a very great variety of material inhomogeneities and intrinsic stress distributions. The evaluation of the complete elastic field is straight forward. It only requires the evaluation of certain derivatives of the potential functions, given in [24].

Finally, we need to take into account the curvature of the surfaces in order to its effect on the resulting contact pressure distribution [40]. As the theoretical approach would not find enough space in this short note, the author will publish the necessary details elsewhere. However, the interested reader may derive the results presented here by comparing the solutions of the Laplace equation in Cartesian and Paraboloidal coordinates.

2.3. The Extension of the Oliver and Pharr Method to Analyze Nanoindentation Data to Layered Materials and Time Dependent Mechanical Behavior

Oliver and Pharr [7] have shown that the force removal curve from elasto-plastic deformations with a Berkovich indenter can be described by a power function:

$$F = C \cdot (h - h_0)^m \tag{13}$$

Applying now the concept of the effective indenter, as shown in Figure 2, one can easily deduce that such an unloading curve can be connected with an Indenter of the shape.

$$Z(r) = B \cdot r^n \tag{14}$$

with:

$$
\begin{aligned}
m &= 1 + \frac{1}{n} \\
C &= 2 \cdot E_r \left[\frac{n}{n+1}\right] \cdot \left[\frac{1}{B} \cdot \left(1 - \varepsilon \cdot \frac{n}{n+1}\right)\right]^{\frac{1}{n}} \\
\frac{1}{E_r} &= \frac{1 - v_i^2}{E_i} + \frac{1 - v_s^2}{E_s} \\
\varepsilon &= m \left[1 - \frac{1}{\sqrt{\pi}} \frac{\Gamma\left(\frac{m}{2 \cdot m - 2}\right)}{\Gamma\left(\frac{2 \cdot m - 1}{2 \cdot m - 2}\right)}\right]
\end{aligned}
\tag{15}
$$

The indices *i* and *s* are standing for the indenter and sample, respectively. The evaluation above is based on the well known results of Sneddon [43], which require a linear elastic model.

Figure 2. The effective indenter concept (see: [4]) transferring the theoretically difficult problem of a well defined sharp indenter on (**a**) an elasto-plastically deformed surface with complex shape to (**b**) an effective indenter on a flat surface.

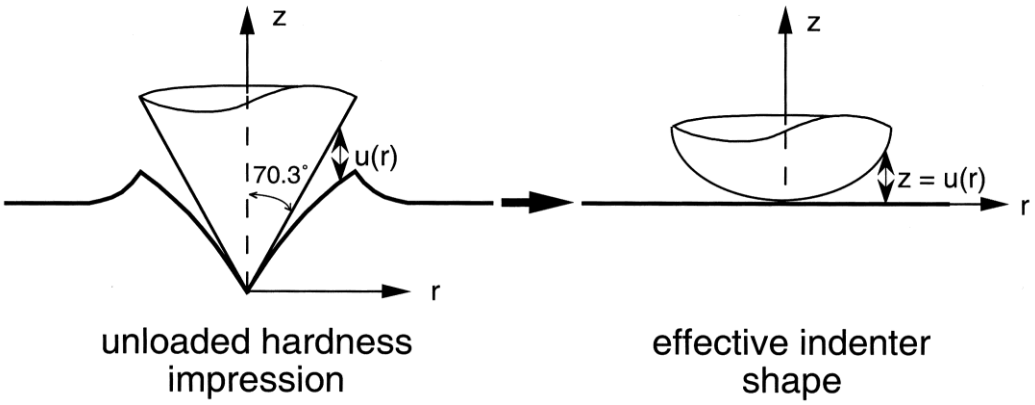

(**a**) (**b**)

For this paper, we need to reformulate the basic contact equation incorporating the plastically deformed surface of the sample with the locally defined shape function (Figure 3):

$$z(r) = B_S \cdot r^n \tag{16}$$

Together with the following approach for the indenter part being in contact with the sample surface of the kind:

$$z'(r) = B_I \cdot r^n \tag{17}$$

we obtain:

$$w(r) + w'(r) = h - (B_I + B_S) \cdot r^n \tag{18}$$

as the new governing contact equation with the parameters $B = B_I + B_S$ and n defining the effective indenter shape $Z(r)$, as given above.

Figure 3. Formulating the contact equation $h = w + z + w' + z'$ with respect to partial plastic deformation z of the sample surface.

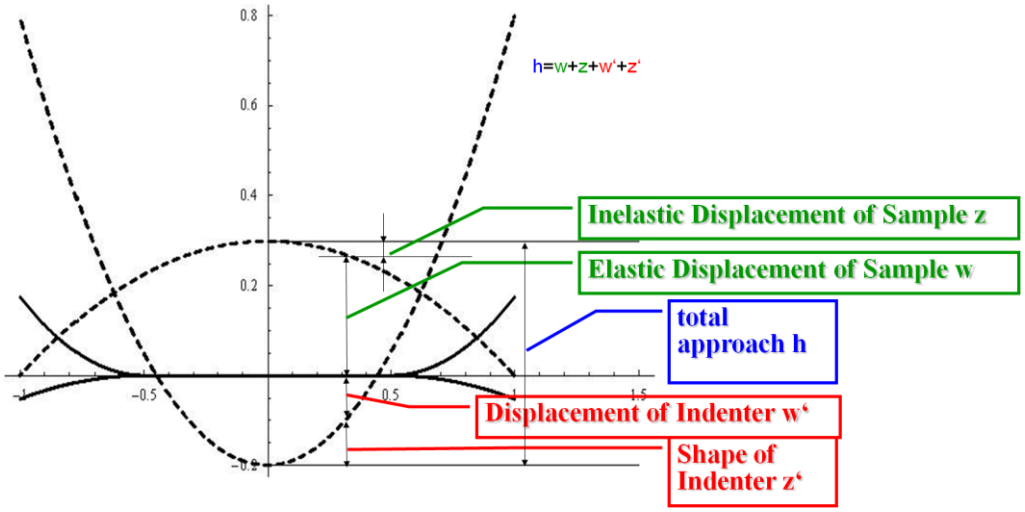

Similarly, also more general effective indenter concepts can be derived, such as this one:

$$\begin{aligned} w_S(r) + w_I(r) &= h - \frac{r^2}{d_0} - \frac{r^4}{d_2} - \frac{r^6}{d_4} - \frac{r^8}{d_6} \\ &= h - r^2\left(\frac{1}{d_0^{\text{Indenter}}} - \frac{1}{d_0^{\text{plastic shape}}}\right) - r^4\left(\frac{1}{d_2^{\text{Indenter}}} - \frac{1}{d_2^{\text{plastic shape}}}\right) \\ &\quad - r^6\left(\frac{1}{d_4^{\text{Indenter}}} - \frac{1}{d_4^{\text{plastic shape}}}\right) - r^8\left(\frac{1}{d_6^{\text{Indenter}}} - \frac{1}{d_6^{\text{plastic shape}}}\right) \\ &= h - r^2\left(c'_0 - c_0\right) - r^4\left(c'_2 - c_2\right) - r^6\left(c'_4 - c_4\right) - r^8\left(c'_6 - c_6\right) \end{aligned} \tag{19}$$

based on a locally paraboloid surface with r-terms r^0, r^2, r^4, r^6, and r^8. The reader might easily recognize the extended Hertzian character [6] of the basic contact equation given above. The simpler Hertzian contact would read:

$$\begin{aligned} w_S(r) + w_I(r) &= h - \frac{r^2}{d_0} \\ &= h - r^2\left(\frac{1}{d_0^{\text{Indenter}}} - \frac{1}{d_0^{\text{plastic shape}}}\right) \\ &= h - r^2\left(c'_0 - c_0\right) \end{aligned} \tag{20}$$

Some of the following examples and discussions will be based on these more general approaches. However, due to the wide use of the power law fit given above we will explicitly concentrate on the power law approach in connection with our practical examples.

In [6] and [24], it is shown how these general contact approaches can be applied and how the complete elastic fields have to be evaluated while the extension to the case of layered materials is been elaborated in [22]. Extension to tilting and lateral loads is given in [6] and [24].

The next extension of need now is a time dependent analysis method for ordinary quasi-static nanoindentation tests (e.g., [2,44] with application [45]). Our approach will be of the following kind [29]:

$$F = C \cdot (h - h_0)^m \quad \rightarrow \quad F = C(t) \cdot (h - h_0(t))^{m(t)} \tag{21}$$

with t denoting the time.

The next step is the introduction of a time dependent material model. Here, for the reason of simplicity, we at first resort to the well known three parameter approach given by a Young's modulus of the following kind $E(t) = E_0 + E_1\exp(-t/\tau)$ (τ is relaxation time).

Now we substitute the time dependent Young's modulus into the function $C(t)$ of Equation (21) and obtain:

$$F = 2 \cdot \left(\frac{1-\nu_i^2}{E_i} + \frac{1-\nu_s^2}{\int_V \left\{ E_{s0} + E_{s1} e^{\frac{-t}{\tau(T_j(r,z),\mu)}} + \vec{r} \cdot E_{s1} e^{\frac{-t}{\tau(T_j(r,z),\mu)}} \frac{t}{\tau^2} \frac{\mathrm{d}\tau}{\mathrm{d}\vec{r}} + \vec{r}^2 \frac{\left(E_{s1} e^{\frac{-t}{\tau(T_j(r,z),\mu)}} \frac{t}{\tau^2} \frac{\mathrm{d}\tau}{\mathrm{d}\vec{r}} \right)^2}{4\left(E_{s0} + E_{s1} e^{\frac{-t}{\tau(T_j(r,z),\mu)}} \right)} \right\} \frac{\mathrm{d}v}{V}} \right)^{-1} \cdot \left[\frac{n}{n+1} \right] \cdot \left(\frac{1}{B} \cdot \left[1 - \varepsilon(n) \cdot \frac{n}{n+1} \right] \right)^{\frac{1}{n}} \cdot (h - h_0)^{\left(1+\frac{1}{n}\right)} \tag{22}$$

Please note that in cases of substantial preloading situations integration with respect to the time t is required.

This makes the classical fit of the three constants h_0, m and C a time dependent 6-parameter fit of h_0, n, B and the material constants E_0, E_1 and τ. It is clear that so many parameters automatically lead to numerical difficulties and instabilities if applied on data not providing sufficient linear independence. Thus, even in the pure visco-plastic case it is strongly suggested to use a variety of unloading curves (3 might be good number) obtained with different unloading speeds or at different maximum loads with similar unloading times.

In cases of time dependent inelastic behavior (like visco-plasticity) or more complex constitutive laws also n, B and h_0 have to be taken as $n(t)$, $B(t)$, $h_0(t)$ making the fit even more complex. The same holds in the visco-elastic case for just h_0 when there are great differences between unloading time and τ (comparable strain rates). The parameters n and B on the other hand are then only geometrical parameters and do not explicitly depend on time. A more detailed derivation and discussion of this extension can be found in [2].

In recent years more and more experimental concepts have been introduced trying to generalize the classical normal indentation process into a multiaxial, combined tilted or twisted contact test [46–51]. In such cases also asymmetric and tilted contact situations need to be manageable. We also need to address the question of how to handle gradient structures, because especially with respect to tribo-protective polymer coatings gradient layers are of use. However, as closed form solutions of this kind are unwieldy and difficult to handle numerically (*cf.* [52,53] regarding elliptical contact situation or [54–56] in the case of a certain gradient structure) or simply do not exist in sufficiently general manner, we prefer the use of load dots as introduced in [57] or [58]. With this approach, a solution of the problem given above can be constructed by combining the superposition of various elastic or visco-elastic spaces as given

in [57] with the introduction of interconnected load dots [57,58]. In our case, the new elastic spaces and loads to be superposed would be differently loaded elastic spaces at suitably chosen time frames with adapted viscose properties along the virtual time-axis. While each frame satisfies a homogeneous elastic problem, the superposition does not necessarily, at least not if the superposition is done in a non-linear way. For some the concept of superposed spaces might be a bit strange, but we remind the reader that in other fields of physics even stranger objects are superposed, such as living and dead cats in quantum mechanics, for instance. This way an approximated solution even for the nonlinear problem given above could be constructed. The method should be demonstrated by the means of interconnected Hertzian load dots (see Appendix) with different contact radii a_i [58] being made time dependent as follows:

$$w = \frac{3}{4}\sum_{i=1}^{N} H_i \frac{\lambda_i(t)}{a_i^3}\left\{\left(2a_i^2 + 2z^2 - r_i^2\right)\sin^{-1}\frac{a_i}{l_{2i}} + \left(l_{2i}^2 - a_i^2\right)^{1/2}\left(\frac{3l_{1i}^2 - 2a_i^2}{a_i}\right)\right\} \tag{23}$$

$$\begin{aligned} u^c &= u + i\cdot v = -\frac{3\alpha}{2}\sum_{i=1}^{N} H_i \frac{\lambda_i(t) r_i e^{i\varphi}}{a_i^3}\left\{\left(a_i^2 - l_{1i}^2\right)^{1/2}\left(1 - \frac{l_{1i}^2 + 2a_i^2}{3r_i^2}\right) + \frac{2a_i^3}{3r_i^2} - z\cdot\sin^{-1}\frac{a_i}{l_{2i}}\right\} \\ l_{1i} &= \frac{1}{2}\left(\sqrt{\left(r_i + a_i\right)^2 + z^2} - \sqrt{\left(r_i - a_i\right)^2 + z^2}\right),\ l_{2i} = \frac{1}{2}\left(\sqrt{\left(r_i + a_i\right)^2 + z^2} + \sqrt{\left(r_i - a_i\right)^2 + z^2}\right) \end{aligned} \tag{24}$$

Here we have used the complex presentation of the lateral displacements with $u^c = u + iv$ (with $i = \sqrt{-1}$, u displacement in x- and v in y-direction, while w gives the displacement in z-direction). The coordinates r_i have to be understood as $r_i = \sqrt{\left(x - x_i\right)^2 + \left(y - y_i\right)^2}$ with x_i and y_i defining the positions of the various load dots. The material functions, respectively, constants H_i and α, are defined through:

$$H_i = \frac{1-\nu^2}{\pi E_i(t)};\quad \alpha = \frac{1-2\nu}{2(1-\nu)} \tag{25}$$

the parameters λ_i have to be fitted to the integral contact equations. They are considered to be only time-dependent, meaning $\lambda_I = \lambda_i(t)$. The reader should note that this approach is just a superposition of Hertzian loads with different contact radii a_i at various positions possibly acting on viscose-elastic spaces being characterized by $H_i = H_i(t)$. From these displacements the strain tensor can be evaluated in the usual manner by using:

$$u_{jk} = \frac{\left(u_{k,j} + u_{j,k}\right)}{2};\quad u_k = \begin{pmatrix} u \\ v \\ w \end{pmatrix} \tag{26}$$

The stress components in the case of linear elasticity can be found using the following identities:

$$\begin{aligned} \sigma_{jk} &= \frac{E}{1+\nu}\left(u_{jk} + \frac{\nu}{1-2\nu}u_{ll}\delta_{jk}\right) \quad \text{with} \quad j,k = x,y,z \equiv 1,2,3 \\ u_{xk} &= \frac{\partial u}{\partial k};\quad u_{yk} = \frac{\partial v}{\partial k};\quad u_{zk} = \frac{\partial w}{\partial k} \end{aligned} \tag{27}$$

In the visco-elastic case applying a 3-parameter Standard Linear Solid model given by a Young's modulus of the following kind $E(t) = E_0 + E_1\exp(-t/\tau)$ and assuming a strain driven loading situation we have instead of Equation (27):

$$\sigma_{jk}(t)=\frac{1}{1+\nu}\left[E_0\left(u_{jk}(t)+\frac{\nu}{1-2\nu}u_{ll}(t)\delta_{jk}\right)+\int_0^t G_{jklm}(t-s)\dot{u}_{lm}(s)\mathrm{d}s\right];\quad \dot{u}_{1m}=\dot{u}_{lm,s}=\frac{\partial u_{lm}}{\partial s} \tag{28}$$

with the tensor of relaxation G_{jkl} being a function of time in the case of linear viscosity. Now, we know, however (e.g., [1,2], and from what was said above), that the assumption of linearity with respect to real life problems is a rather flawed one. In addition, it is almost hopeless to make proper assumption or estimates for the complete tensor function G_{jklm}. Especially in tribological contact situations we will find stress, strain and temperature fields dramatically influencing the tensor function. However, with our inter-atomic based approach from the beginning of the theory section we are in principle able to give a more correct description by the means of our field dependent Young's modulus for the sample:

$$E_{\mathrm{s}}(t)=\int_{\mathrm{V}}\left\{E_{\mathrm{s}0}+\sum_{q=1}^{j}E_{sq}\mathrm{e}^{\frac{-t}{\tau_q}}+\vec{r}\cdot\sum_{q=1}^{j}E_{sq}\mathrm{e}^{\frac{-t}{\tau_q}}\frac{t}{\tau_q^2}\frac{\mathrm{d}\tau_q}{\mathrm{d}\vec{r}}+\vec{r}^{\,2}\frac{\left(\sum_{q=1}^{j}E_{sq}\mathrm{e}^{\frac{-t}{\tau_q}}\frac{t}{\tau_q^2}\frac{\mathrm{d}\tau_q}{\mathrm{d}\vec{r}}\right)^2}{4\left(E_{\mathrm{s}0}+\sum_{q=1}^{j}E_{sq}\mathrm{e}^{\frac{-t}{\tau_q}}\right)}\right\}\frac{\mathrm{d}\,v}{V} \tag{29}$$

This results in

$$\sigma_{jk}=\frac{1}{1+\nu}\left[\begin{array}{l}E_0\left(u_{jk}+\frac{\nu}{1-2\nu}u_{ll}\delta_{jk}\right)+\\ \int_0^t\left(\dot{U}_{jk}+\frac{\nu}{1-2\nu}\dot{U}_{ll}\delta_{jk}\right)\int_V\left(\begin{array}{l}\sum_{q=1}^{j}E_{sq}\mathrm{e}^{\frac{s-t}{\tau_q}}+\vec{r}\cdot\sum_{q=1}^{j}E_{sq}\mathrm{e}^{\frac{s-t}{\tau_q}}\frac{t-s}{\tau_q^2}\frac{\mathrm{d}\tau_q}{\mathrm{d}\vec{r}}\\ +\vec{r}^{\,2}\frac{\left(\sum_{q=1}^{j}E_{sq}\mathrm{e}^{\frac{s-t}{\tau_q}}\frac{t-s}{\tau_q^2}\frac{\mathrm{d}\tau_q}{\mathrm{d}\vec{r}}\right)^2}{4\left(E_{s0}+\sum_{q=1}^{j}E_{sq}\mathrm{e}^{\frac{s-t}{\tau_q}}\right)}\end{array}\right)\frac{\mathrm{d}v}{V}\mathrm{d}s\end{array}\right];$$
$$\dot{U}_{jk}=\dot{U}_{jk,s}=\frac{\partial U_{jk}}{\partial s} \tag{30}$$

In some cases it is more convenient to use a continuous relaxation function, which results in:

$$\sigma_{jk}=\frac{1}{1+\nu}\left[\begin{array}{l}E_0\left(u_{jk}+\frac{\nu}{1-2\nu}u_{ll}\delta_{jk}\right)+\\ \int_0^t\left(\dot{U}_{jk}+\frac{\nu}{1-2\nu}\dot{U}_{ll}\delta_{jk}\right)\int_V\left(\begin{array}{l}\int_0^\infty E_s(\tau)\mathrm{e}^{\frac{s-t}{\tau}}\mathrm{d}\tau\\ +\vec{r}\cdot\int_0^\infty\left(\frac{\mathrm{d}E_s(\tau)}{\mathrm{d}\tau}+E_s(\tau)\frac{t-s}{\tau^2}\right)\frac{\mathrm{d}\tau}{\mathrm{d}\vec{r}}\mathrm{e}^{\frac{s-t}{\tau}}\mathrm{d}\tau\\ +\vec{r}^{\,2}\frac{\left(\int_0^\infty\left(\frac{\mathrm{d}E_s(\tau)}{\mathrm{d}\tau}+E_s(\tau)\frac{t-s}{\tau^2}\right)\frac{\mathrm{d}\tau}{\mathrm{d}\vec{r}}\mathrm{e}^{\frac{s-t}{\tau}}\mathrm{d}\tau\right)^2}{4\left(E_{s0}+\int_0^\infty E_s(\tau)\mathrm{e}^{\frac{s-t}{\tau}}\mathrm{d}\tau\right)}\end{array}\right)\frac{\mathrm{d}v}{V}\mathrm{d}s\end{array}\right];$$
$$\dot{U}_{jk}=\dot{U}_{jk,s}=\frac{\partial U_{jk}}{\partial s} \tag{31}$$

With the assumption of adiabatic temperature fields following the shear field, such an approach appears to be manageable, but its solution strongly depends on the actual shear distribution (*cf.* [2]). For the reason of simplicity, we will continue the evaluation with the phenomenological SLS-approach, which should be applicable *in situ* ations without significant temperature fields [2].

We start as follows:

$$\sigma_{jk} = \frac{1}{1+\nu}\left[E_0\left(u_{jk} + \frac{\nu}{1-2\nu}u_{ll}\delta_{jk}\right) + E_1\int_0^t\left(\dot{U}_{jk} + \frac{\nu}{1-2\nu}\dot{U}_{ll}\delta_{jk}\right)\mathrm{e}^{-\frac{t-s}{\tau}}\mathrm{d}s\right];$$
$$\dot{U}_{jk} = \dot{U}_{jk,s} = \frac{\partial U_{jk}}{\partial s} \tag{32}$$

We see that by performing the following substitution underneath the time integrals:

$$\int_0^t (...)E_1\mathrm{e}^{-\frac{t-s}{\tau}}\mathrm{d}s \Rightarrow \int_0^t (...)\int_V \left[\begin{array}{l}\sum_{q=1}^{j} E_{sq}\mathrm{e}^{\frac{s-t}{\tau_q}} + \vec{r}\times\sum_{q=1}^{j} E_{sq}\mathrm{e}^{\frac{s-t}{\tau_q}}\frac{t-s}{\tau_q^2}\frac{\mathrm{d}\tau_q}{\mathrm{d}\vec{r}} \\ +\vec{r}^{\,2}\dfrac{\left(\sum_{q=1}^{j} E_{sq}\mathrm{e}^{\frac{s-t}{\tau_q}}\frac{t-s}{\tau_q^2}\frac{\mathrm{d}\tau_q}{\mathrm{d}\vec{r}}\right)^2}{4\left(E_{s0}+\sum_{q=1}^{j} E_{sq}\mathrm{e}^{\frac{s-t}{\tau_q}}\right)}\end{array}\right]\frac{\mathrm{d}v}{V}\mathrm{d}s \tag{33}$$

we are always able to switch back to the more general form.

Further on, in order to have maximum flexibility for the construction of a great variety of contact situations combined with sufficient simplicity to keep the model analytical, we introduce the method of time dependent Hertzian load dots as outlined in the Appendix.

The approach has the advantage, that the evaluation of the complete elastic field for the whole body would only be a question of summing up a series of potentially time dependent Hertzian fields. In addition, the solution can easily be extended to layered materials [28]. In order to fit the model even better to the real test or application one might also make the constants c_i time-dependent. This, of course, requires reevaluation of the Integral in Equation (33) but caused by the distribution structure (properties of the Dirac delta function) in the integrand any such additional time-dependency would be very easy to handle. In addition one could go for extended Hertzian load dots instead of Hertzian ones (e.g., [6]), incorporate tilting, twisting and lateral loads, defects, and intrinsic stresses as done in [12,39,40]. Then the method is also applicable to asymmetric scratch- or tribo-like contact situations.

2.4. Theory for the Physical Scratch and/or Tribological Test

The governing contact equation and stress distributions for more general loading conditions as occurring during tests like scratch and pin on disc have already been given in the Section “the effective indenter concept”. The evaluation of the complex stress and strain fields for these tests is elaborated in the references given there. However, as these evaluations are rather cumbersome and lengthy, the reader is also referred to a software package performing such calculations in an automated and quick manner [28].

It should explicitly be pointed out that knowledge of the complete stress and strain field is essential for a proper failure characterization (scratch) or wear mechanism analysis (tribo). An example is presented in the figures below. There, Figures 4 and 5 present the evolution of the stress field for the von Mises and the normal stress, respectively in the case of a typical scratch test performed on hard coatings on steel substrates (*cf.* [10–12] regarding material and test parameters). Figure 6 shows the typical failure mechanism as being observed in the tests shown in the tests presented in Figures 4 and 5. For more information, the reader is referred to [12].

Figure 4. The evolution of von-Mises stress during the scratch test shown at three measurement positions: (**a**) at the beginning of the scratch test, (**c**) in the moment of L_C failure, and (**b**) in between. The black cross hairs indicate the location of the maximum.

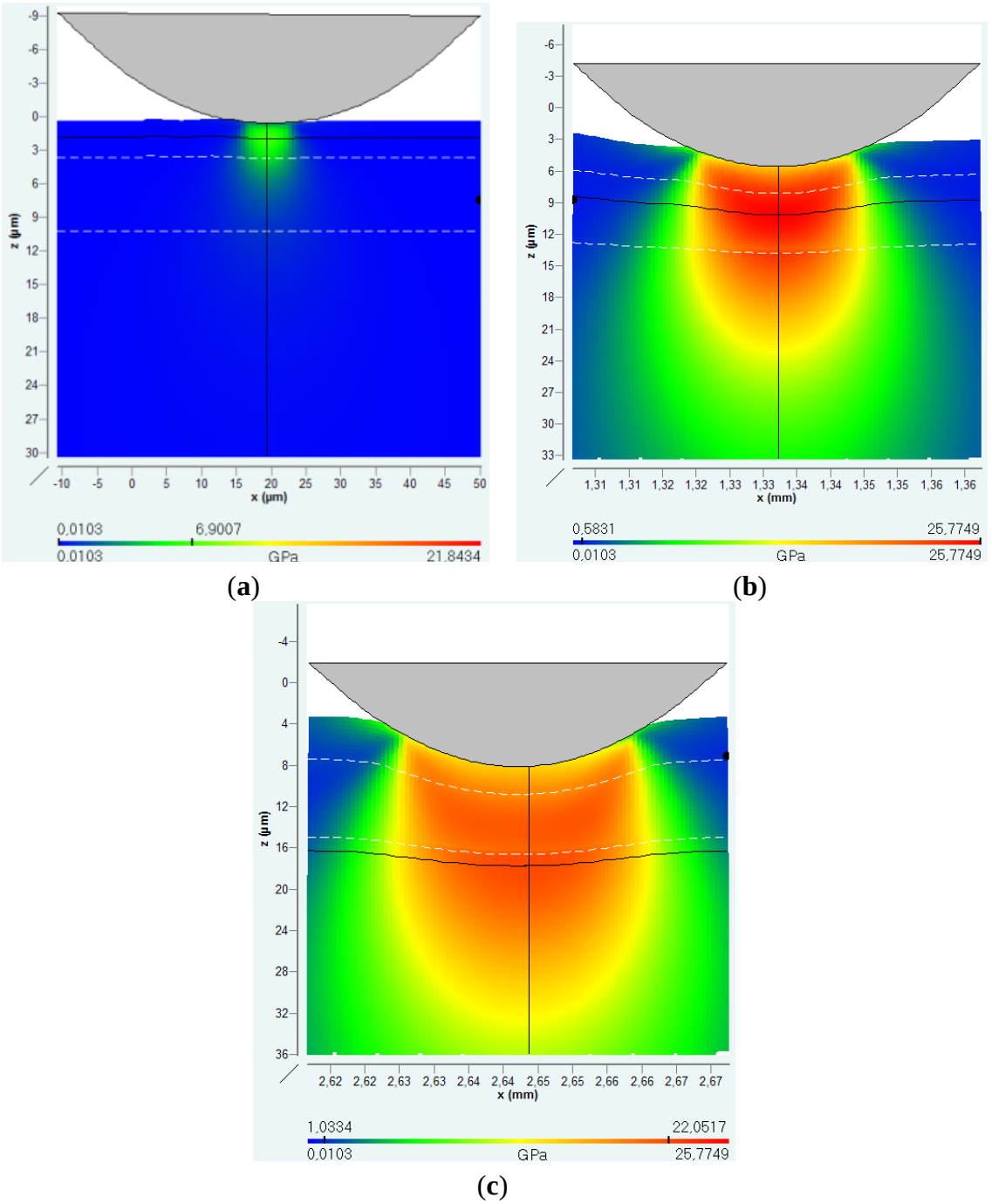

Figure 5. The evolution of normal stress in scratch direction illustrated at three measurement positions: (**a**) at the beginning of the scratch test, (**c**) in the moment of L_C failure, and (**b**) in between. The black cross hairs indicate the location of maximum tensile stress.

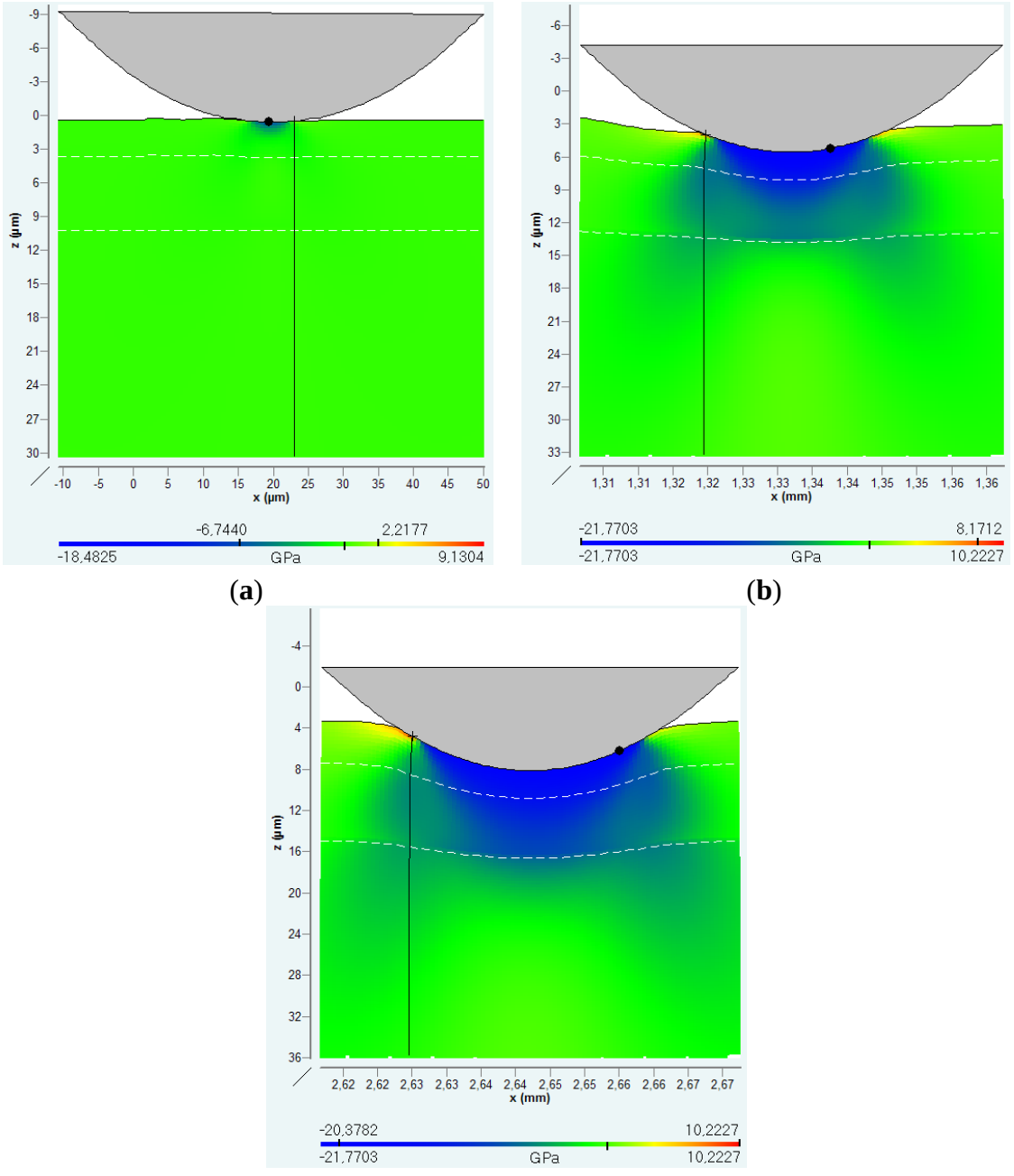

Hence, only such a physical analysis of mechanical contact measurements like instrumented indentations, scratch, and tribo-tests enable one to find out why a surface structure fails under certain loading conditions. These results provide indications on how the investigated coating or surface structure can be improved (structurally be optimized of adapted with respect to the material selection).

Figure 6. Illustrative scheme of the failure mechanism (**a**) and an optical graph of the post-scratch surface (**b**) in which the corresponding L_C position is marked by the red dashed line [12].

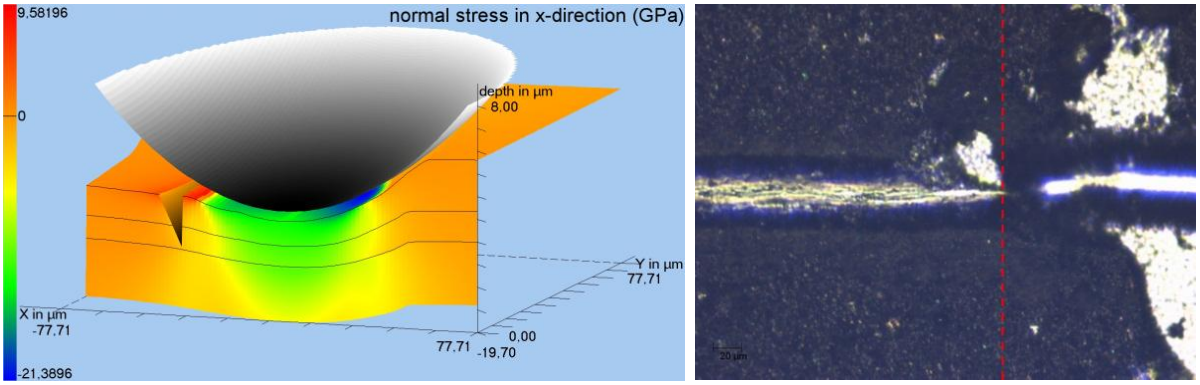

(**a**) (**b**)

From Quasi-Static Experiments and Parameters to Dynamic Wear, Fretting and Tribological Tests

Now we need to establish the relationship between quasi-static characteristics, like hardness, yield strength, Young's modulus, *etc.*, and highly dynamic characteristics like wear, fretting and other tribological processes and effects.

First of all, it must be understood that within the concept of this approach the process of wear, fretting or a general tribological process is a to be considered as a multi-physical, multi body (asperity) ensemble of contact situations (called load dots, *cf.* [57,58]) with each having its own geometry, load conditions (including tilting, normal, lateral, twisting loads, plus temperature fields caused by internal or external friction) and—in complex cases with debris—also multiple time scales, meaning various parts of the global tribological contact are running in their own speed. Of course, we will then also have to take temperature effects into account. These are often coupling back into the mechanical properties and time dependent material behavior (*cf.* Section "The extension of the Oliver and Pharr method to analyze nanoindentation data to layered materials and time dependent mechanical behavior"). However, the mathematics of partial differential equations does provide an interesting short cut here. It is due to the similarity of the governing differential equations that by having found the solution for the contact problem also the temperature field or any other "diffusion-like" problem can be considered solved. Thus, the layered solution for any diffusion problem can be constructed from the elastic solution by letting the Poisson's ratio go to infinity, which leads to perfectly non-singular field solution for the diffusion problem in question.

In addition to that, the connection between non-physical parameters (like hardness) towards wear is not the intention of the paper. In fact, there is no such connection—strictly speaking. Something not generic, like hardness, simply cannot, not generally, be extended or applied to a dynamic process like wear. Hardness, after all, is a mixed parameter. There are so many things contributing to hardness that, in general, it is not clear what effects affecting the hardness are also influencing wear (and in what manner), for instance. Thus, yield strength, critical fracture stresses, fracture toughness (energy loss caused by fracture propagation), in short, parameters, which could clearly be connected to certain stress fields and stress components, are much better suited to also interpret and discuss tribological effects.

We are now concentrating on some questions that often pop up in connection with tribological tests and observations.

Where is the role of debris particles?

They are just adding up to the complex jumble of contact situations mentioned above.

How are strain-rate or even more general time-dependent effects taken into account?

This is usually been done by applying time-functional dependencies for the mechanical parameters. However, as shown in [2], in the presence of inhomogenous fields possibly influencing the mechanical parameters the resulting governing equations are becoming highly nonlinear. This can either be treated by the means of piecewise X-parameter models or by solving the nonlinear governing system of equations with time-stress- and strain-dependent material parameters (*cf.* Section "The extension of the Oliver and Pharr method to analyze nanoindentation data to layered materials and time dependent mechanical behavior"). First principle derived basics are given in [2].

How are intrinsic stresses been taken into account?

Intrinsic stresses are just adding to the external stresses (and strain) fields and lead to a subsequent shift of onset of inelastic behavior, be it fracture, plastic flow, or phase transition. Therefore it is very important to know and consider intrinsic stresses as accurately as possible. Here, "accurately" explicitly means that intrinsic stresses are usually not homogeneously distributed but also present a complex field adding up to the deformation field coming from external loading situations.

Due to their importance we here refer to a more comprehensive elaboration about the modeling of these stresses especially in connection with external loads (e.g., [41,57,59]).

How can the many faces of wear and tribo effects be incorporated into one theoretical apparatus?

The straight forward answer would be: By decomposition limits extracted from first principle approaches. Hereby, the most general way would be to extract decomposition limits from the first principle approaches as described in [2]. These limits have to be compared with the deformation fields obtained in the multiple complex contact model describing our tribo, fretting or wear experiments, where nonlinear effects, as described in [1] and [2], should not be neglected. Even though we will demonstrate how this, in principle, can be done within the procedure-plan below, it is eminent that such a procedure is not necessarily fit for daily or even industrial use. Therefore, we also need a phenomenological description of the physics behind tribo-effects in an as general as possible manner.

At first, we explicitly point out, that wear or any other tribological effect cannot be connected by a simple k_d-value or any other scalar value (e.g., Archard's law) to the deformation or stress field. This is by far too simple and not general enough. Instead, in the simplest (linear) case, the tribo-effect is a tensor, coupling with wear-moduli to every deformation field component in a fully covariant manner. Consequently, any tribo-process can be generalized as:

$$\begin{aligned} tribo-effect_{ij} &= k^{\sigma}{}_{ijkl}\,\sigma^{kl} + k^{\varepsilon}{}_{ijkl}\,\varepsilon^{kl} + k^{u}{}_{ijkl}\,u^k u^l + \sum_{\chi=1}^{N} k^{S_\chi}\delta_{ij}S_n \\ &+ k^{\sigma}{}_{ijklmn}\,\sigma^{kl}\sigma^{mn} + k^{\varepsilon}{}_{ijklmn}\,\varepsilon^{kl}\varepsilon^{mn} + k^{u}{}_{ijklmn}\,u^k u^l u^m u^n + \sum_{\chi=1}^{N} k2^{S_\chi}\delta_{ij}S_n^2 \\ &+ k^{\sigma}{}_{ijklmnop}\,\sigma^{kl}\sigma^{mn}\sigma^{op} + k^{\varepsilon}{}_{ijklmnop}\,\varepsilon^{kl}\varepsilon^{mn}\varepsilon^{op} + k^{u}{}_{ijklmnop}\,u^k u^l u^m u^n u^o u^p + \sum_{\chi=1}^{N} k3^{S_\chi}\delta_{ij}S_n^3 + \ldots \end{aligned} \tag{34}$$

It should be made clear, that the sensitivity of a given tribological pairing towards certain components of the deformation field strongly depends on the initial failure mechanisms driving, respectively dominating the process. Thus, we will probably have a higher dependency on the deviatoric stress field (given by the second invariant or the von Mises stress) where the tribology is mainly determined by plastic flow. The examples given in the paper are apparently governed by these effects. In those cases however, where we expect fracture to dominate the tribological process, wear components coupling to the normal stresses or directed shear stresses will increase over the other components of the tribo- or wear tensor. Here, we can easily deduce that mode I fracture would lead to higher components connected with the normal stresses, while mode II and mode III fracture driven tribology requires shear dominated wear tensors. In some cases also pressure driven phase transitions could be responsible for the observed tribology. Then the tribo- or wear tensor will have dominant terms coupling to the first invariant of the stress field, because this gives the pressure field multiplied by three.

Here we will concentrate mainly on linear dependencies [first line in Equation (34)], where we used the following denotations: $k^{xx}{}_{ijkl}$-tensors are tensors coupling to the various field values or tensors like the stress σ^{kl}, strain ε^{kl}, displacement-vector u^i or scalar values S_n, like free or distortion energy strain work *etc.* The symbol δ_{ij} is the Kroenecker symbol. In some cases, like simple wear tests for instance, it should be sufficient to consider only the stresses:

$$tribo-effect_{ij} \equiv w_{ij} = k_{ijkl}\ \sigma^{kl} \tag{35}$$

Wherefrom the scalar wear-depth h_w has to be evaluated via:

$$h_w = w_{ij}\ n^i\ n^j \tag{36}$$

with n^i denoting the surface normal unit vector.

We have to point out explicitly, that all the stresses, strains, vectors, energies *etc.* as being used in Equation (34) are field values and not just numbers. Thus, they are to be understood as functions of the coordinates. However, in the end and in order to have an apparatus one can compare with real experiments one prefers to obtain numbers for the tribo-effect or wear instead of complicated functions. Thus, for many applications the components of the k-tensors must even have operational character. For example, if considering the maximum of a certain stress it might be of great importance where exactly that maximum lays within the material. Let us assume a blunt indenter contact situation and a tribo-effect being dominated by fatigue caused by the total shear. In such a case, we will always find the von Mises stress maximum underneath the surface. It seems reasonable in this situation to assume that the amount of destruction respectively the mass of worn off material is not just connected with the absolute value of the von Mises stress maximum σ_{vM}, but also its distance z to the surface respectively the contact centre $\left|\vec{r}\right|$. One could formulate this as:

$$w_{ij} = \delta_{ij}\left(k_{dvM}\sigma_{vM}\cdot \mathrm{e}^{-\lambda_k \vec{r}\cdot\vec{r}}\right) \tag{37}$$

with λ_k being yet another parameter in addition to the linear k_{dvM} characterizing the wear performance in dependency of the von Mises stress distribution. We point out that, in using the local load acting on a certain contacted surface point, we have the following local wear depth:

$$h_w = w_{ij}\sigma^{ij}_{surface} = \delta_{ij}\left(k_{dvM}\sigma_{vM}\cdot \mathrm{e}^{-\lambda_k \vec{r}\cdot\vec{r}}\right)\sigma^{ij}_{surface} = \sigma^{zz}_{surface}\left(k_{dvM}\sigma_{vM}\cdot \mathrm{e}^{-\lambda_k \vec{r}\cdot\vec{r}}\right) \tag{38}$$

Using the quantum mechanical marking to note operators we could use the following generalization for an operational form of (34):

$$tribo-effect_{ij} = \hat{k}^{\sigma}_{ijkl}\ \sigma^{kl} + \hat{k}^{\varepsilon}_{ijkl}\ \varepsilon^{kl} + \hat{k}^{u}_{ijkl}\ u^{k}u^{l} + \sum_{n=1}^{N} \hat{k}^{S_n}\delta_{ij}S_n \tag{39}$$

For the wear-example given above we can formulate this as:

$$tribo-effect_{ij} \equiv w_{ij} = \hat{k}_{ijkl}\ \sigma^{kl} \quad \equiv \quad \delta_{ij}\left(k_{dvM}\sigma_{vM}\cdot \mathrm{e}^{-\lambda_k \vec{r}\cdot\vec{r}}\right) \tag{40}$$

As we can see, the Archard's law given with a scalar wear coefficient k_d by the simple relation $h_w = k_d \times \sigma^{33}$ is nothing but a rather dramatic simplification of Equation (35) being possible wherever either the stress is dominated by its normal component in the surface normal direction (here, we named it σ^{33}) or where the coefficient tensor k_{ijkl} is zero except for those components coupling to the normal surface stress σ^{33}, which would then read:

$$h_w = w_{ij}\ n^i\ n^j = k_{ijkl}\ \sigma^{kl} n^i\ n^j = k_{33kl}\ \sigma^{kl} \simeq k_{3333}\sigma^{33} \equiv k_d\sigma^{33} \tag{41}$$

We can deduce now that for complex contact conditions, where the stress tensor is fully set and no component is dominant against all the others, one should be rather careful with the assumption of having the wear-tensor being of the most simple, Archard's-law-like kind

$$k_{33kl} = \begin{pmatrix} 0 & 0 & 0 \\ 0 & 0 & 0 \\ 0 & 0 & k_{3333} \end{pmatrix}$$

One should also take the other stresses into account and investigate their possible influence regarding the resulting global wear, which, in this case, has to be taken as the sum over all stress-components in connection with the wear-tensor:

$$h_w = k_{33kl}\ \sigma^{kl} = k_{3311}\sigma^{11} + k_{3322}\sigma^{22} + k_{3333}\sigma^{33} + 2\left(k_{3312}\sigma^{12} + k_{3313}\sigma^{13} + k_{3323}\sigma^{23}\right) \tag{42}$$

Here, we have made use of the symmetry of the stress tensor, also requiring a symmetric wear-tensor.

We also point out, that in the general law as given above in Equation (35) the hydrostatic (sphere) and deviatoric stress parts are distinguishable. Such a simplified law might read:

$$tribo-effect_{ij} \equiv w_{ij} = \overbrace{k_{dShear\_ij}\left(\sigma_{ij} - \frac{1}{3}\delta_{ij}\sigma_{ll}\right)}^{shear\ part} + \overbrace{\delta_{ij}k_{dSphere}\frac{1}{3}\sigma_{ll}}^{pressure\ part} \tag{43}$$

or even simpler, and further scalarized:

$$w_{ij} = \delta_{ij}\left(k_{dvM}\sigma_{vM} + k_{dH}\sigma_H\right) \tag{44}$$

with σ_{vM}, σ_H, denoting the von Mises and the hydrostatic stress, respectively.

3. Experimental Section

Within a variety of examples the procedure or parts of it have already been applied [7–14]. Here now, we want to deepen the analysis and discussion by the means of these previous examples and try to

improve the simulation by taking nonlinear and temperature effects into account. An illustrative elaboration of the procedure is been given in [60].

It was shown in [13] and [14] that the use of an operator-like wear or tribo-law as introduced in the section above brought some improvement regarding the comparison with experimental data. It was also shown and elaborated that the analytical method as outlined here has the big advantage of delivering quasi "in-sight-views" about the deformation fields, strains, stresses, and so on, of the surfaces subjected to such tribology tests. Due to the completely analytical character of the tools used the calculation usually is extremely fast and robust. This way weak spots within the material composition can be found more easily and efficiently. Subsequently, also optimizing surface systems towards a better tribo-performance could be done quicker and still more accurately.

We have demonstrated this on the wear track example presented in [13] and [14], where an oscillating wear test with a spherical indenter had been performed. The indenter was sliding forth and back along a certain track thereby wearing off material. In [60] (Figures 11–19) it was shown how the theoretical models mirrors the gradual "digging" in of the indenter with increasing cycle number and the subsequent evolution of the stress field for a variety of stress components. The evaluation was performed with the software FilmDoctor [28].

Still, there had been deviations from the experiment which could not been explained in a satisfactory manner. However, it was already mentioned (*cf.* [13,14] and also see [2]) that nonlinear or temperature effects could play a role. Especially with respect to temperature one would expect to see some influence as the tests performed were reciprocating wear tests where a spherical indenter is performing an oscillatory sliding movement over the, in some cases coated, sample surface. Here, the friction will automatically lead to a temperature increase. With such an increase of temperature, we expect a change of the mechanical parameters, especially Young's modulus and yield strength.

Simply assuming such an influence and incorporating it into the wear simulation as described in [13] and [14] by the means of a Young's modulus function of the kind given in Equation (29) thereby assuming a temperature dependency of the relaxation time or viscosity like:

$$\tau = \eta / E_1 = \frac{\eta_0 \mathrm{e}^{W_A/(k_B T)}}{E_1} \tag{45}$$

We hope to result into a better fit of our wear or tribo model to the experimental data. Using a similar dependency for the yield strength *Y* as we did for the Young's modulus and adapting our wear-law (40) such that the wear should increase with decreasing *Y*, we set:

$$tribo-effect_{ij} \equiv w_{ij} = \hat{k}_{ijkl}\ \sigma^{kl} \quad \equiv \quad \delta_{ij}\left(k_{dvM} \frac{\sigma_{vM}}{Y(T)} \cdot \mathrm{e}^{-\lambda_k \vec{r}\cdot\vec{r}} \right) \tag{46}$$

Here, we need to pay attention to the fact, that with having a temperature dependent Young's modulus by the means of Equations (29) and (45) we also result in a temperature dependency for the von Mises stress maximum and its position. This makes the evaluation of Equation (46) relatively complicated and we therefore restrict ourselves here to the task of finding a temperature function $T(n)$ with n denoting the number of cycles or oscillations of the indenter which would fit the real wear data significantly better than an assumed constant temperature. For both examples, we had at hand [13,14] and we received significantly better fit results in this way. Interestingly, the best function $T(n)$ to use was of the kind

$T(n) = c_0 \times \tanh(c_1 \times n)$ which simply coincides with a temperature rise at the beginning of the test and reaching a plateau value after only a view cycles. This surprisingly simple result does not only have some beauty with respect to its low number of free parameters, but also can easily be understood by the interpretation of the indenter producing friction and leading to a temperature increase until a state of equilibrium is reached where the temperature in the vicinity of the contact does not increase any further. The results are shown in Figures 7 and 8.

Figure 7. Comparison of various wear laws with the experimental data (*cf.* text in Section 3). The data have been reused from [13].

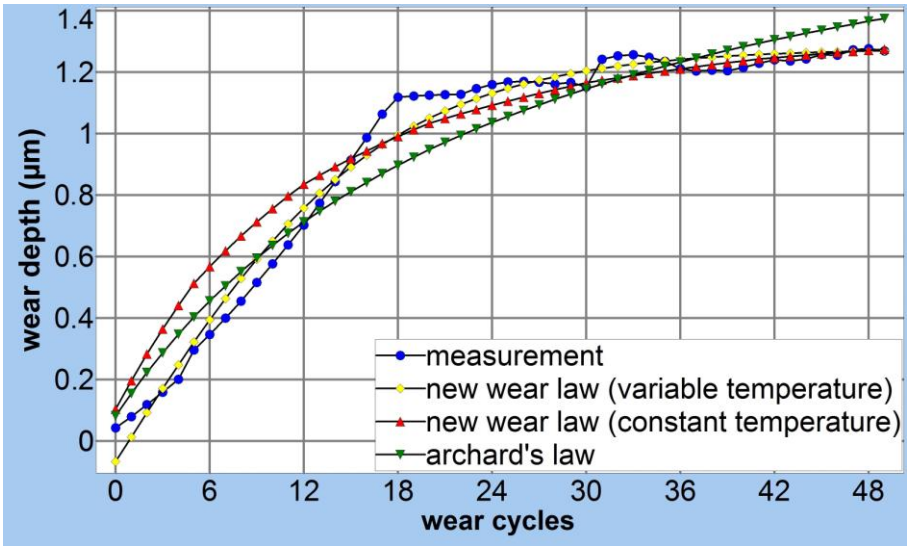

Figure 8. Comparison of various wear laws with the experimental data (*cf.* text in Section 3). The data have been reused from [14].

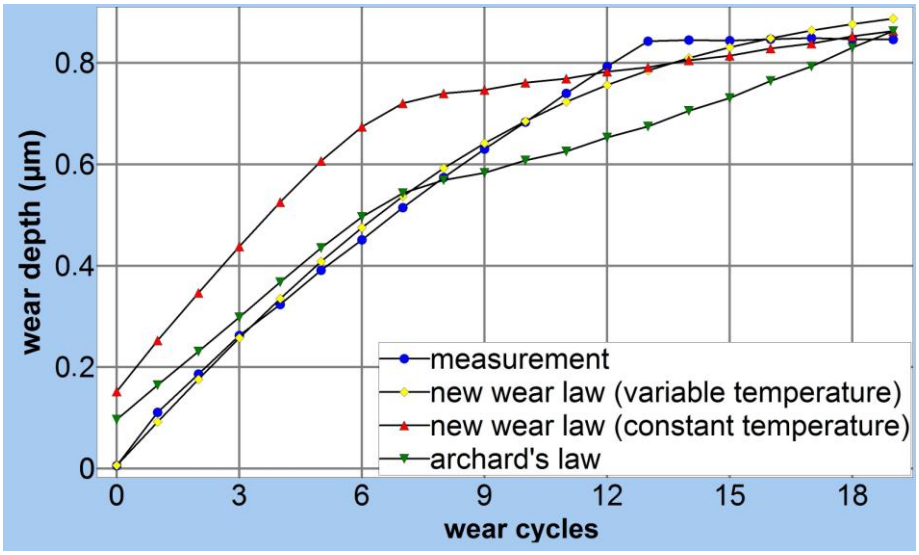

It should be pointed out that, especially in scratch and wear tests, often, effects like work hardening, grain refinement, intrinsic stress, and general defect accumulation lead to significant material parameter changes during the test. In principle the model allows to account for such effects simply by making the material parameters which are affected by such effects dependent on the evolution of the test. Such a

dependency could either be steered via time, wear cycle or any other evolutional parameter counting the test progress. Within the examples given in Figures 7 and 8 we only found enough experimental significance for the temperature coupling into the material properties leading to a parameter dependency for the Young's modulus and the yield strength. As elaborated above, this dependency was accounted for by using the wear cycle number n as evolutional parameter.

More examples including better illustration of the intermediate steps as well as a more comprehensive description of the experiments are published elsewhere (e.g., [10–14,60]).

4. Conclusions

By combining the global incremental wear model with the concept of the effective indenter, the extended Hertzian approach and a layered half space solution for contact problems with rather arbitrary combinations of normal, lateral and tilting loads a general, quick and powerful wear model has been created.

Inversion of the model makes it fit for parameter identification and optimization problems.

Further, adding first principle models, like effective interatomic interaction potentials allows a deeper understanding of those failure mechanisms being responsible for wear results observable in practical tests.

Temperature effects had been taken into account by allowing the temperature to couple into the mechanical properties Young's modulus and yield strength.

Possible subsequent time dependent material behavior leads to a relatively complex inhomogeneous Young's modulus distribution which must be taken into account if one aims for a better simulation of wear experiments.

The analytical method as outlined here has the advantage of delivering quasi "in-sight-views" about the deformation fields, strains, stresses, and so on, of the surfaces subjected to such tribology tests. Due to the completely analytical character of the tools used the calculation usually is extremely fast and robust. This way weak spots within the possibly layered material composition can be found more easily and efficiently. Subsequently, also optimizing surface systems towards a better tribo-performance could be done quicker and still more accurately.

Acknowledgements

This work was partially funded through the European Metrology Research Programme (EMRP) Project IND05 MeProVisc. The EMRP is jointly funded by the EMRP participating countries within EURAMET and the European Union.

Appendix

Arbitrary Hertzian Load Dots

By introducing Hertzian load-dots as:

$$w_i = \frac{3}{4}\frac{\begin{pmatrix}\lambda_i(t)\\ \Lambda_i(t)\end{pmatrix}}{a_i^3}\left\{\left(2a_i^2+2z^2-r_i^2\right)\sin^{-1}\frac{a_i}{l_{2i}}+\left(l_{2i}^2-a_i^2\right)^{1/2}\left(\frac{3l_{1i}^2-2a_i^2}{a_i}\right)\right\}\equiv\begin{pmatrix}\lambda_i\\ \Lambda_i\end{pmatrix}\tilde{w}_i;\quad i=1,2,...N \qquad \text{(A1)}$$

$$u_i^c = -\frac{3\alpha}{2}\frac{\begin{pmatrix}\lambda_i(t)\\ \Lambda_i(t)\end{pmatrix} r_i \mathrm{e}^{i\varphi}}{a_i^3}\left\{\left(a_i^2 - l_{1i}^2\right)^{1/2}\left(1 - \frac{l_{1i}^2 + 2a_i^2}{3r_i^2}\right) + \frac{2a_i^3}{3r_i^2} - z\cdot\sin^{-1}\frac{a_i}{l_{2i}}\right\} \equiv \begin{pmatrix}\lambda_i\\ \Lambda_i\end{pmatrix}\tilde{u}_i^c; \quad i = 1,2,...N \tag{A2}$$

$$\tilde{u}_{ijk} = \frac{\left(\tilde{u}_{ik,j} + \tilde{u}_{ij,k}\right)}{2}; \quad \tilde{u}_{ik} = \begin{pmatrix}\tilde{u}\\ \tilde{v}\\ \tilde{w}\end{pmatrix}_i; \quad \tilde{u}_i^c = \tilde{u}_i + i\cdot\tilde{v}_i; \quad \begin{matrix} i = 1,2,...N \\ j,k = 1,2,3\end{matrix} \tag{A3}$$

we obtain the rather simple expression for the stress tensor with index *i*:

$$\sigma_{ijk} = \frac{\left(\tilde{u}_{ijk} + \frac{\nu}{1-2\nu}\tilde{u}_{ill}\delta_{jk}\right)}{1+\nu}\left[E_0\lambda_i(t) + E_1\int_0^t \dot{\Lambda}_i(s)\mathrm{e}^{-\frac{t-s}{\tau}}\mathrm{d}s\right]; \quad \dot{\Lambda}_i = \dot{\Lambda}_{i,s} = \frac{\partial\Lambda_i}{\partial s}; \quad \begin{matrix} i = 1,2,...N \\ j,k = 1,2,3\end{matrix} \tag{A4}$$

Applying an exponential approach for the $\Lambda_i(t) = \lambda_i(t)$ reading $\lambda_i = c_i\cdot e^{-\frac{t}{\tau_i}}$ which here only is chosen as an example we obtain the solution:

$$\sigma_{ijk} = \frac{\left(\tilde{u}_{ijk} + \frac{\nu}{1-2\nu}\tilde{u}_{ill}\delta_{jk}\right)}{1+\nu}\left[E_0 c_i e^{-\frac{t}{\tau_i}} - c_i\tau E_1\frac{e^{-\frac{t}{\tau}} - e^{-\frac{t}{\tau_i}}}{\tau - \tau_i}\right]; \quad \begin{matrix} i = 1,2,...N \\ j,k = 1,2,3\end{matrix} \tag{A5}$$

Now we derive the situation for a stress driven deformation state. Again applying the 3-parameter model together with our simple load-dot approach we have:

$$u_{jk} = \frac{1}{E}\left((1+\nu)\sigma_{jk} - \nu\,\sigma_{ll}\delta_{jk}\right) \quad with \quad j,k = 1,2,3; \quad u_{xk} = \frac{\partial u}{\partial k}; \quad u_{yk} = \frac{\partial v}{\partial k}; \quad u_{zk} = \frac{\partial w}{\partial k} \tag{A6}$$

$$u_{ijk} = \left((1+\nu)\widehat{\sigma}_{ijk} - \nu\,\widehat{\sigma}_{ill}\delta_{jk}\right)\left[\frac{\gamma_i(t)}{E_0} + \left(\frac{1}{E_0 + E_1} - \frac{1}{E_0}\right)\int_0^t \dot{\Gamma}_i(s)\mathrm{e}^{-\frac{E_0}{E_0+E_1}\frac{t-s}{\tau}}\mathrm{d}s\right] \tag{A7}$$

$$\dot{\Gamma}_i = \dot{\Gamma}_{i,s}; \quad \begin{matrix} i = 1,2,...N \\ j,k = 1,2,3\end{matrix}$$

where the stresses $\widehat{\sigma}$ are now to be understood as

$$\sigma_{ijk} = \begin{pmatrix}\gamma_i(t)\\ \Gamma_i(t)\end{pmatrix}\widehat{\sigma}_{ijk} = \frac{\begin{pmatrix}\gamma_i(t)\\ \Gamma_i(t)\end{pmatrix}}{1+\nu}\left(\widehat{u}_{ijk} + \frac{\nu}{1-2\nu}\widehat{u}_{ill}\delta_{jk}\right); \quad \widehat{u}_{ixk} = \frac{\partial\widehat{u}_i}{\partial k}; \quad \widehat{u}_{iyk} = \frac{\partial\widehat{v}_i}{\partial k}; \quad \widehat{u}_{izk} = \frac{\partial\widehat{w}_i}{\partial k} \tag{A8}$$

$$\widehat{w}_i = \frac{3}{4}\frac{1}{a_i^3}\left\{\left(2a_i^2 + 2z^2 - r_i^2\right)\sin^{-1}\frac{a_i}{l_{2i}} + \left(l_{2i}^2 - a_i^2\right)^{1/2}\left(\frac{3l_{1i}^2 - 2a_i^2}{a_i}\right)\right\} = \frac{\tilde{w}_i}{\begin{pmatrix}\lambda_i\\ \Lambda_i\end{pmatrix}}; \quad i = 1,2,...N \tag{A9}$$

$$\widehat{u}_i^c = -\frac{3\alpha}{2}\frac{r_i e^{i\varphi}}{a_i^3}\left\{\left(a_i^2 - l_{1i}^2\right)^{1/2}\left(1 - \frac{l_{1i}^2 + 2a_i^2}{3r_i^2}\right) + \frac{2a_i^3}{3r_i^2} - z\cdot\sin^{-1}\frac{a_i}{l_{2i}}\right\} = \frac{\tilde{u}_i^c}{\begin{pmatrix}\lambda_i\\ \Lambda_i\end{pmatrix}}; \quad i = 1,2,...N \tag{A10}$$

$$\widehat{u}_{ijk}=\frac{\left(\widehat{u}_{ik,j}+\widehat{u}_{ij,k}\right)}{2};\quad \widehat{u}_{ik}=\begin{pmatrix}\widehat{u}\\ \widehat{v}\\ \widehat{w}\end{pmatrix}_i;\quad \widehat{u}_i^c=\widehat{u}_i+i\cdot\widehat{v}_i;\quad \begin{matrix}i=1,2,...N\\ j,k=1,2,3\end{matrix} \tag{A11}$$

Generalized with respect to field dependent mechanical properties and sticking to a 3-parameter potential interaction the Equation (A7) would read:

$$\begin{aligned}C(t)=&\frac{1}{E_0}+\left(\frac{1}{E_0+E_1}-\frac{1}{E_0}\right)\mathrm{e}^{-\frac{E_0}{E_0+E_1}\frac{t}{\tau}}-\vec{r}\cdot\left(\frac{E_1}{\left(E_0+E_1\right)^2}\right)\mathrm{e}^{-\frac{E_0}{E_0+E_1}\frac{t}{\tau}}\frac{t}{\tau^2}\frac{\mathrm{d}\tau}{\mathrm{d}\vec{r}}\\&+\vec{r}\cdot\vec{r}\,\frac{\left(\left(\frac{E_1}{\left(E_0+E_1\right)^2}\right)\mathrm{e}^{-\frac{E_0}{E_0+E_1}\frac{t}{\tau}}\frac{t}{\tau^2}\frac{\mathrm{d}\tau}{\mathrm{d}\vec{r}}\right)^2}{4\left(\frac{1}{E_0}+\left(\frac{1}{E_0+E_1}-\frac{1}{E_0}\right)\mathrm{e}^{-\frac{E_0}{E_0+E_1}\frac{t}{\tau}}\right)}\end{aligned} \tag{A12}$$

Extension to discrete or continuous retardation gives:

$$u_{ijk}=\left((1+\nu)\widehat{\sigma}_{ijk}-\nu\,\widehat{\sigma}_{ill}\delta_{jk}\right)\int_V\left[\begin{aligned}&\frac{\gamma_i(t)}{E_0}+\int_0^t\sum_{q=1}^n\frac{1}{E_q}\dot{\Gamma}_i(s)\left(1-\mathrm{e}^{-\frac{t-s}{\tau_{Eq}}}\right)\mathrm{d}s\\&+\vec{r}\cdot\int_0^t\sum_{q=1}^n\frac{1}{E_q}\dot{\Gamma}_i(s)\mathrm{e}^{-\frac{t-s}{\tau_{Eq}}}\frac{t-s}{{\tau_{Eq}}^2}\frac{\mathrm{d}\tau}{\mathrm{d}\vec{r}}\mathrm{d}s\\&+\vec{r}\cdot\vec{r}\int_0^t\frac{\left(\sum_{q=1}^n\frac{1}{E_q}\dot{\Gamma}_i(s)\mathrm{e}^{-\frac{t-s}{\tau_{Eq}}}\frac{t-s}{{\tau_{Eq}}^2}\frac{\mathrm{d}\tau}{\mathrm{d}\vec{r}}\right)^2}{4\left(\frac{1}{E_0}+\sum_{q=1}^n\frac{1}{E_q}\dot{\Gamma}_i(s)\left(1-\mathrm{e}^{-\frac{t-s}{\tau_{Eq}}}\right)\right)}\mathrm{d}s\end{aligned}\right]\frac{\mathrm{d}v}{V} \tag{A13}$$

$$u_{ijk}=\begin{pmatrix}(1+\nu)\widehat{\sigma}_{ijk}-\\ \nu\,\widehat{\sigma}_{ill}\delta_{jk}\end{pmatrix}\int_V\left[\begin{aligned}&\frac{\gamma_i(t)}{E_0}+\int_0^t\int_0^\infty\frac{1}{E(\tau)}\left(1-\mathrm{e}^{-\frac{t-s}{\tau}}\right)\mathrm{d}\tau\,\dot{\Gamma}_i(s)\mathrm{d}s+\\&\vec{r}\cdot\int_0^t\int_0^\infty\frac{1}{E(\tau)}\left(\frac{t-s}{\tau^2}\mathrm{e}^{-\frac{t-s}{\tau}}-\frac{\left(1-\mathrm{e}^{-\frac{t-s}{\tau}}\right)}{E(\tau)}\frac{\mathrm{d}E(\tau)}{\mathrm{d}\tau}\right)\frac{\mathrm{d}\tau}{\mathrm{d}\vec{r}}\mathrm{d}\tau\,\dot{\Gamma}_i(s)\mathrm{d}s+\\&\vec{r}\cdot\vec{r}\int_0^t\frac{\dot{\Gamma}_i(s)\left(\int_0^\infty\frac{1}{E(\tau)}\left(\frac{t-s}{\tau^2}\mathrm{e}^{-\frac{t-s}{\tau}}-\frac{\left(1-\mathrm{e}^{-\frac{t-s}{\tau}}\right)}{E(\tau)}\frac{\mathrm{d}E(\tau)}{\mathrm{d}\tau}\right)\frac{\mathrm{d}\tau}{\mathrm{d}\vec{r}}\mathrm{d}\tau\right)^2}{4\left(\frac{1}{E_0}+\int_0^\infty\frac{1}{E(\tau)}\left(1-\mathrm{e}^{-\frac{t-s}{\tau}}\right)\mathrm{d}\tau\right)}\mathrm{d}s\end{aligned}\right]\frac{\mathrm{d}v}{V} \tag{A14}$$

For reasons of simplicity however, we will here proceed with the gradient free simple SLS-model. Together with the normalization condition and the total normal load $p = p(t)$ one obtains

$$\begin{aligned} p(t) &= \int_0^{2\pi}\int_0^{a_{\max}} \sigma_{zz}(r,\varphi,z)\big|_{z=0} r\mathrm{d}r\mathrm{d}\varphi \equiv \int_0^{2\pi}\int_0^{a_{\max}} \sigma_{zz0}(r,\varphi) r\mathrm{d}r\mathrm{d}\varphi \\ &= 2\pi\int_0^{a_{\max}} \sigma_{zz0}(r) r\mathrm{d}r = \sum_{i=1}^{N}\left[E_0 c_i \mathrm{e}^{-\frac{t}{\tau_i}} - c_i \tau E_1 \frac{\mathrm{e}^{-\frac{t}{\tau}} - \mathrm{e}^{-\frac{t}{\tau_i}}}{\tau - \tau_i} \right] \end{aligned} \tag{A15}$$

for the strain driven case, while one derives in the stress driven situation with $\Gamma_i(t) = \gamma_i(t)$:

$$\begin{aligned} p(t) &= \int_0^{2\pi}\int_0^{a_{\max}} \sigma_{zz}(r,\varphi,z)\big|_{z=0} r\mathrm{d}r\mathrm{d}\varphi \equiv \int_0^{2\pi}\int_0^{a_{\max}} \sigma_{zz0}(r,\varphi) r\mathrm{d}r\mathrm{d}\varphi \\ &= 2\pi\int_0^{a_{\max}} \sigma_{zz0}(r) r\mathrm{d}r = 2\pi\sum_{i=1}^{N}\left[\int_0^{a_i} \gamma_i(t)\widehat{\sigma}_{izz0}(r) r\mathrm{d}r \right] = \sum_{i=1}^{N}\gamma_i(t) \end{aligned} \tag{A16}$$

Both cases are relatively easy whenever there will be no change of the contact area during the evolution of the deformation time being considered. In most practical applications however, this is not the case. Concentrating on contact experiments we can often assume that they are load controlled. However, due to the complex mixed stress states underneath the contact zone, there are also strain effects involved and it is not clear yet how to take these into account. Therefore Equations (A6)–(A11) and (A16) are applicable but need to be extended with respect to strain driving effects (e.g., [2], Appendix). There are several options how to make the contact area evolvable during the time slot being considered. One could either change the number of load dots being taken into account respectively contributing to the whole contact or make the contact radii a_i time dependent. As the latter way immediately leads to much more complicated integrals we are going for the first option not by the apparent simple way of changing the total load-dot number N but by introducing Heaviside distributions to the $\gamma_i(t)$ (or respectively the $\lambda_i(t)$ in the strain drive case) as follows:

$$\gamma_i(t) = c_i\left[\Phi\left(t - t_{ion}\right) - \Phi\left(t - t_{ioff}\right)\right]; \quad \dot{\Gamma}_i(t) = \dot{\gamma}_i(t) = c_i\left[\delta\left(t - t_{ion}\right) - \delta\left(t - t_{ioff}\right)\right]; \quad t_{ion} < t_{ioff} \tag{A17}$$

with

$$\Phi(t) = \begin{cases} 0 \text{ for } t \le 0 \\ 1 \text{ for } t > 0 \end{cases} \tag{A18}$$

and δ giving the Dirac delta distribution. With this approach the integration in Equation (A7) can be performed easily as Equation (A19).

For many cases in contact applications we are facing mixed stress-strain driven conditions requiring a combination of Equations (A4) and (A7). Choosing a sufficiently high number of load dots N one can approximate any displacement (time dependent effective indenter shape) of symmetry of revolution. By placing the load dots in a non concentric manner also asymmetric contact situation can be described.

$$u_{ijk} = \left((1+\nu)\widehat{\sigma}_{ijk} - \nu\,\widehat{\sigma}_{ill}\delta_{jk}\right)\left[\begin{array}{l}\dfrac{c_i\left[\Phi\left(t-t_{ion}\right)-\Phi\left(t-t_{ioff}\right)\right]}{E_0} \\ +\left(\dfrac{1}{E_0+E_1}-\dfrac{1}{E_0}\right)\displaystyle\int_0^t c_i\left[\delta\left(s-s_{ion}\right)-\delta\left(s-s_{ioff}\right)\right]e^{-\frac{E_0}{E_0+E_1}\frac{t-s}{\tau}}\,ds\end{array}\right]$$

$$= c_i\left((1+\nu)\widehat{\sigma}_{ijk} - \nu\,\widehat{\sigma}_{ill}\delta_{jk}\right)\left[\begin{array}{l}\dfrac{1}{E_0}\begin{cases}0 & t \le t_{ion} \\ 1 & t_{ion} < t \le t_{ioff} \\ 0 & t_{ioff} < t\end{cases} \\ +\left(\dfrac{1}{E_0+E_1}-\dfrac{1}{E_0}\right)\begin{cases}0 & t \le t_{ion} \\ e^{-\frac{E_0}{E_0+E_1}\frac{t-t_{ion}}{\tau}} & t_{ion} < t \le t_{ioff} \\ e^{-\frac{E_0}{E_0+E_1}\frac{t-t_{ion}}{\tau}} - e^{-\frac{E_0}{E_0+E_1}\frac{t-t_{ioff}}{\tau}} & t_{ioff} < t\end{cases}\end{array}\right] \quad \text{(A19)}$$

Conflicts of Interest

The author declares no conflict of interest.

References

1. Schwarzer, N. Short note on the effect of pressure induced increase of Young's modulus. *Philos. Mag.* **2012**, *92*, 1631–1648.
2. Schwarzer, N. From interatomic interaction potentials via Einstein field equation techniques to time dependent contact mechanics. *Mater. Res. Express* **2014**, *1*, doi:10.1088/2053-1591/1/1/015042.
3. Bolshakov, A.; Oliver, W.C.; Pharr, G.M. An Explanation for the Shape of Nanoindentation Unloading Curves based on Finite Element Simulation. *MRS Symp. Proc*. **1994**, *356*, doi:10.1557/PROC-356-675.
4. Pharr, G.M.; Bolshakov, B. Understanding nanoindentation unloading curves. *J. Mater. Res.* **2002**, *17*, 2660–2671.
5. Schwarzer, N.; Pharr, G.M. On the evaluation of stresses during nanoindentation with sharp indenters. *Thin Solid Films* **2004**, *469–470*, 194–200.
6. Schwarzer, N. The extended Hertzian theory and its uses in analysing indentation experiments. *Philos. Mag.* **2006**, *86*, 5153–5767.
7. Oliver, W.C.; Pharr, G.M. An improved technique for determining hardness and elastic modulus using load and displacement sensing indentation experiments. *J. Mat. Res.* **1992**, *7*, 1564–1583.
8. Schwarzer, N.; Chudoba, T.; Pharr, G.M. On the evaluation of stresses for coated materials during nanoindentation with sharp indenters. *Surf. Coat. Technol*. **2006**, *200*, 4220–4226.
9. Schwarzer, N.; Chudoba, T.; Richter, F. Investigation of ultra thin coatings using nanoindentation. *Surf. Coat. Technol.* **2006**, *200*, 5566–5580.
10. Fuchs, M.; Favaro, G. Physical characterization of coated surfaces—Part I: instrumented indentation. Available online: http://www.csm-instruments.com/en/Physical-characterization-of-coated-surfaces-Part-I-%3A-Instrumented-Indentation (accessed on 17 April 2014).

11. Fuchs, M.; Favaro, G. Physical characterization of coated surfaces—Part II: scratch test. Available online: www.csm-instruments.com/en/Physical-characterization-of-coated-surfaces-Part-II-%3A-Scratch-Test (accessed on 17 April 2014).
12. Schwarzer, N.; Duong, Q.-H.; Bierwisch, N.; Favaro, G.; Fuchs, M.; Kempe, P.; Widrig, B.; Ramm, J. Optimization of the scratch test for specific coating designs. *Surf. Coat. Technol.* **2011**, *206*, 1327–1335.
13. Gies, A.; Chudoba, T.; Schwarzer, N.; Becker, J. Influence of the coating structure of a-C:H-W coatings on their wear-performance: A theoretical approach and its practical confirmation. In Proceedings of International Conference on Metallurgical Coatings and Thin Films (ICMCTF), San Diego, CA, USA, 29 April–3 May 2013.
14. Liskiewicz, T.; Beake, B.; Schwarzer, N.; Davies, M. Short note on improved integration of mechanical testing in predictive wear models. In Proceedings of International Conference on Metallurgical Coatings and Thin Films (ICMCTF), San Diego, CA, USA, 29 April–3 May 2013.
15. Schwarzer, N. Is ultra-hardness possible—A brief feasibility study. Available online: http://www.siomec.de/ultra-hard-coatings (accessed on 17 April 2014).
16. Lie, M.; Chen, N.X. Möbius inversion transform for diamond-type materials and phonon dispersions. *Phys. Rev. B***1995**, *52*, 997–1003.
17. Dick, T. Cailletaud, G. Fretting modelling with a crystal plasticity model of Ti6Al4V. *Comput. Mater. Sci.* **2006**, *38*, 113–125.
18. Guilemany, J.M.; Dosta, S.; Miguel, J.R. The enhancement of the properties of WC-Co HVOF coatings through the use of nanostructured and microstructured feedstock powders. *Surf. Coat. Technol.* **2006**, *201*, 1180–1190.
19. Hegadekatte, V.; Huber, N.; Kraft, O. Modeling and simulation of wear in a pin on disc tribometer. *Tribol. Lett.* **2006**, *24*, 51–60.
20. Holm, R. *Electric Contacts*; Almqvist and Wiksells Boktryxkeri AB: Uppsala, Sweden, 1946.
21. Holmberg, K.; Matthews, A. *Coatings Tribology*, 2nd ed.; Springer: Amsterdam, The Netherlands, 2009.
22. Schwarzer, N. Arbitrary load distribution on a layered half space. *ASME J. Tribol.* **2000**, *122*, 672–681.
23. Chudoba, T.; Herrmann, K. Verfahren zur Ermittlung der realen Spitzenform von VICKERS- und BERKOVICH-Eindringkörpern. *HTM Härt. Mitt.* **2001**, *56*, 258–264. (In German)
24. Schwarzer, N. Elastic surface deformation due to indenters with arbitrary symmetry of revolution. *J. Phys. D* **2004**, *37*, 2761–2772.
25. Schwarzer, N. Analysing nanoindenation unloading curves using Pharr's concept of the effective indenter shape. *Thin Solid Films* **2006**, *494*, 168–172.
26. Richter, F.; Herrmann, M.; Molnar, F.; Chudoba, T.; Schwarzer, N.; Keunecke, M.; Bewilogua, K.; Xiang, X.W.; Boyen, H.-G.; Ziemann, P. On the evaluation of stresses in coated materials during nanoindentation with sharp indenters Substrate influence in Young's modulus determination of thin films by indentation methods: Cubic boron nitride as an example. *Surf. Coat. Technol.* **2006**, *201*, 3577–3587.

27. Puschmann, R.; Schwarzer, N.; Richter, F.; Frühauf, S.; Schulz, S.E. An applicable concept for the indentation of thin porous films. In Proceedings of the NanoMech 5, Hückelhoven, Germany, 7–9 September 2004; pp. 1–6.
28. *FilmDoctor*; Saxonian Institute of Surface Mechanics: Ummanz, Germany, 2010.
29. Fischer-Cripps, A.C. A simple phenomenological approach to nanoindentation creep. *Mater. Sci. Eng. A* **2004**, *385*, 74–82.
30. François, D.; Pineau, A.; Zaoui, A. *Mechanical Behaviour of Materials*; Springer, Dordrecht, The Netherlands, 2012.
31. *ISO 20502:2005 Fine Ceramics (Advanced Ceramics, Advanced Technical Ceramics)—Determination of Adhesion of Ceramic Coatings by Scratch Testing*; ISO: Geneva, Switzerland, 2005.
32. *ASTM C1624 Standard Test Method for Adhesion Strength and Mechanical Failure Modes of Ceramic Coatings by Quantitative Single Point SCRATCH Testing*; ASTM International: West Conshohocken, PA, USA, 2010.
33. *O&PfC*; Saxonian Institute of Surface Mechanics: Ummanz, Germany, 2010.
34. *ISA*; Saxonian Institute of Surface Mechanics: Ummanz, Germany, 2010.
35. *SSA*; Saxonian Institute of Surface Mechanics: Ummanz, Germany, 2010.
36. *TestOptimizer*; Saxonian Institute of Surface Mechanics: Ummanz, Germany, 2013.
37. Ehlert, J.; Batz, W.J.; Der Einfluss von Druck und Temperatur auf die effektive Viskosität in geschmierten kontra-formen Kontakten. *Rheol. Acta* **1976**, *15*, 356–364. (In German)
38. Phillips, R.B. *Crystals, Defects and Microstructures*; Cambridge University Press: Cambridge, UK, 2001.
39. Schwarzer, N. Some basic equations for the next generation of surface testers solving the problem of pile-up, sink-in and making area-function-calibration obsolete. *J. Mater. Res.* **2009**, *24*, 1032–1036.
40. Schwarzer, N. Basic equations for the next generation of surface testers for the case of an elastic indenter and a layered samples. Saxionian Institute of Surface Mechanics. Available online: http://www.siomec.de/pub/2008/001 (accessed on 17 April 2014).
41. Schwarzer, N. Intrinsic stresses—Their influence on the yield strength and their measurement via nanoindentation. Saxonian Institute of Surface Mechanics. Available online: http://www.siomec.de/pub/2007/001 (accessed on 17 April 2014).
42. Schwarzer, N. Modelling of contact problems of rough surfaces. Saxonian Institute of Surface Mechanics. Available online: http://www.siomec.de/pub/2007/007 (accessed on 17 April 2014).
43. Sneddon, I.N. The relation between load and penetration in the axisymmetric Boussinesq problem for a punch of arbitrary profile. *Int. J. Eng. Sci.* **1965**, *3*, 47–57.
44. Schwarzer, N. Analyse und Simulation der mechanischen Eigenschaften beschichteter Polymere unter Berücksichtigung der meist zeitabhängigen Materialparameter. In Proceedings of the V2011 Industrieausstellung & Workshop-Woche, Dresden, Germany, 17–20 October 2011; pp. 96–101. (In German)
45. Kohl, J.G.; Randall, N.X.; Schwarzer, N.; Ngo, T.T.; Shockley, J.M.; Nair, R.P. An investigation of scratch testing of silicone elastomer coatings with a thickness gradient. *J Appl. Polym. Sci.* **2012**, *124*, 2978–2986.

46. Lucas, B.N.; Hay, J.L.; Oliver, W.C. Using multi-dimensional contact mechanics experiments to measure Poisson's ratio of porous low-k films. *J. Mater. Res.* **2004**, *19*, 58–65.
47. Molnár, O. Investigations of Nanoindentation Data Obtained by the Combination of Normal and Mixed (Normal and Lateral) Forces. Ph.D. Thesis, Technical University of Chemnitz, Chemnitz, Germany, 2010. (In German)
48. Karniychuk, M. Combination of Lateral and Normal Forces for Investigation of Mechanical Properties and Tribological Behaviour of Bulk and Coated Materials on the Micro-Scale. Ph.D. Thesis, Technical University of Chemnitz, Chemnitz, Germany, 2006. (In German)
49. Chudoba, T.; Linss, V.; Karniychuk, M.; Richter, F. Lateral force–displacement measurements—A new technique for the investigation of mechanical surface properties. *Surf. Coat. Technol.* **2005**, *200*, 315–320.
50. Gies, A.; Schwarzer, N.; Becker, J.; Rudigier, H. *Untersuchung der mechanischen Eigenschaften von DLC-Schichtsystemen mittels Nanoindentation und deren Modellierung*; Tagungsband der ThGOT: Jena, Germany, 2010; pp. 104–109. (In German)
51. Schwarzer, N. Coating design due to analytical modelling of mechanical contact problems on multilayer systems. In Proceedings of the International Conference on Metallurgical Coatings and Thin Films (ICMCTF), San Diego, CA, USA, 10–14 April 2000; pp. 397–402.
52. Fabrikant, V.I. Several elliptical punches on an elastic half space. *J. Appl. Mech.* **1986**, *53*, 390–394.
53. Argatov, I.I. Asymptotic models of contact interaction among elliptic punches on a semiclassical foundation. *Int. Appl. Mech.* **2006**, *42*, 67–83.
54. Popov, G.I. Axisymmetric contact problem for an elastic inhomogeneous half-space in the presence of cohesion. *Prikl. Math. I Mech.* **1973**, *37*, 1109–1116. (In Russian)
55. Fabrikant, V.I. *Application of Potential Theory in Mechanics: A Selection of New Results*; Kluver Academic Publishers: Dordrecht, The Netherlands, 1989.
56. Rostovtsev, N.A. On certain solutions of an integral equation of the theory of a linearly deformable foundation. *Prikl. Math. I Mech.* **1961**, *25*, 164–168. (In Russian)
57. Schwarzer, N. Modelling of the mechanics of thin films using analytical linear elastic approaches. Available online: www.siomec.de/pub/2007/013 and http://archiv.tu-chemnitz.de/pub/2004/0077 (accessed on 17 April 2014).
58. Schwarzer, N. Effect of lateral displacement on the surface stress distribution for cone and sphere contact. *Phil. Mag.* **2006**, *86*, 5231–5237.
59. Schwarzer, N.; Richter, F. On the determination of film stress from substrate bending: Stoney's formula and its limits. Online Archive of the Technical University of Chemnitz, Chemnitz, Germany. Available online: http://archiv.tu-chemnitz.de/pub/2006/0011 (accessed on 17 Arpil 2014).
60. Schwarzer, N. Endlessly touchable—the next generation of surface and coating optimization. Saxionian Institute of Surface Mechanics. Availiable online: http://www.siomec.de/pub/2013/001 (accessed on 17 April 2014).